공학석사학위논문

에틸렌옥사이드-카보네이트 공중합체를 기반으로 하는 준상호침투형 가교구조의 고분자 전해질 제조 및 리튬이차전지로의 응용

Organic/Inorganic Hybrid Semi-Interpenetrating Network Electrolytes Based on Poly(ethylene oxide-*co*-ethylene carbonate) for All-Solid-State Lithium Batteries

2014년 2월

서울대학교 대학원

화학생물공학부

권 수 지

에틸렌옥사이드-카보네이트 공중합체를 기반으로 하는 준상호침투형 가교구조의 고분자 전해질 제조 및 리튬이차전지로의 응용

Organic/Inorganic Hybrid Semi-Interpenetrating Network Electrolytes Based on Poly(ethylene oxide-*co*-ethylene carbonate) for All-Solid-State Lithium Batteries

지도교수 이 종 찬

이 논문을 공학석사 학위논문으로 제출함.

2014년 2월

서울대학교 대학원

화학생물공학부

권 수 지

권수지의 공학석사학위논문을 인준함.

2014년 2월

위 원 장 _____(印)

부위원장 _____ (印)

위 원 _____(印)

Abstract

Organic/Inorganic Hybrid Semi-Interpenetrating Network Electrolytes Based on Poly(ethylene oxide-*co*-ethylene carbonate) for All-Solid-State Lithium Batteries

Su-Jee Kwon

Polymer Chemistry

Department of Chemical & Biological Engineering

Seoul National University

Organic/inorganic hybrid semi-interpenetrating network electrolytes (HIPE) based on poly(ethylene oxide-*co*-ethylene carbonate) (PEOEC) have been developed for all-solid-state lithium battery applications. In comparison to poly(ethylene oxide) (PEO)-based electrolytes, the salient features of the PEOEC electrolytes are the amorphous nature and high dielectric constant, which provide enhanced ionic conductivity. The organic/inorganic hybrid network matrix in

HIPE is composed of different contents of photo-cross-linked octa-functional POSS acrylate (OA-POSS) and ethoxylated trimethylolpropane triacrylate (ETPTA). The effect of OA-POSS on solid-state electrolyte properties of the HIPE is investigated in terms of dimensional stability, thermal behavior, and ionic conductivity. Due to the presence of the rigid and bulky POSS moiety, the HIPE exhibits improvement in ionic conductivity, along with enhanced dimensional stability. The high capacity and good cycle performance of lithium battery with the HIPE demonstrates the feasibility of applying the HIPE to solid-state electrolytes for all-solid-state lithium batteries.

Keywords: All-Solid-State Batteries, Organic/Inorganic Hybrid Materials, Polyhedral Oligomeric Silsesquioxane(POSS), Semi-Interpenetrating Network, Poly(ethylene oxide-*co*-ethylene carbonate)

List of Tables

List of Schemes

List of Figures

dependence of ionic conductivities of L-HIPE10 and H-HIPE10.

Figure 9. Linear Sweep Voltamograms of Stainless Steel Electrodes in L-HIPE10 with $LiSO_3CF_3$ at 25 ^oC and 60 ^oC.

Figure 10. (a) Charge-Discharge Curves and (b) Discharg capacity *vs.* Cycle Behaviors of All-Solid-State Li / L-HIPE10 (with $LiSO_3CF_3$) / V_2O_5 cell measured at 60 ^oC.

List of Supporting Figures

List of Contents

1. Introduction

As lithium rechargeable batteries begin to be applied as a power source for electric or hybrid electric vehicles, the battery safety will become increasingly important.[1, 2] The safety issues of lithium batteries are closely related to the use of liquid electrolytes, which have several drawbacks such as leakage, volatility, spontaneous combustion of the electrolytes, limited temperature range of operation, and lack of mechanical stability.[3] To surmount these shortcomings of liquid electrolytes, solid polymer electrolytes (SPEs) have received considerable attentions due to their advantages, including non-volatility, low flammability, chemical and electrochemical stability, and widely tunable shape conformations.[1, 4, 5] To date, poly(ethylene oxide) (PEO) coupled with lithium salt has been the most frequently and thoroughly studied polymer electrolyte.[6-8] However, the PEO cannot be applied as a practical SPE, because it has comparatively low ionic conductivity (~10^{-7} S cm^{-1} at room temperature) owing to the existence of crystalline domains that interfere with lithium ion conduction.[9, 10] In addition, the

PEO is known to have low dielectric constant that it cannot allow an effective dissociation of the lithium salt, resulting in a large amount of contact ion pairs or higher ion aggregates.[11-14] This could also cause a detrimental effect on the ionic conductivity.

The incorporation of polar subunits into PEO-based polymeric structures has been studied to enhance the ionic conductivity of PEO-based electrolytes by increasing the dielectric constant and decreasing the crystallinity of PEO.[15, 16] Previously, we have reported the synthesis of poly(ethylene oxide-*co*-ethylene carbonate) (PEOEC) by ring opening polymerization of ethylene carbonate.[17] It was found that the PEOEC has an amorphous state due to the polar carbonate units linked by ether moieties. This unique structural feature of PEOEC can provide enhanced ionic conductivity when employed as a polymer host for SPEs. Jeon et al. studied a pore-filling electrolyte based on a porous membrane filled with the PEOEC electrolyte.[18, 19] However, the application of the pore-filling electrolyte could be limited due to the complicated preparation process. Elmér et al. also described the application of PEOEC for SPEs by utilizing cross-linked

polymeric structures, although the ionic conductivity was below 10^{-5} S cm^{-1} at room temperature.[20] Therefore, a simple, effective approach to prepare PEOEC-based SPEs with high ionic conductivity needs to be suggested. In addition, the ionic conductivity behavior of PEOEC electrolytes should be further investigated, because the effects of carbonate units and molecular weight of PEOEC on the ionic conductivity has not been elucidated in detail.

It is desirable for SPEs to exhibit sufficient dimensional stability to separate the electrode as well as their high ionic conductivity. Although the PEOEC electrolyte shows enhanced ionic conductivity, it is normally in a wax state so it does not have sufficient dimensional stability. In order to achieve a balance between the ionic conductivity and dimensional stability of SPEs, several strategies such as composite polymer electrolytes,[21, 22] block copolymer electrolytes,[23, 24] pore-filling polymer electrolytes,[25] and semi-interpenetrating network (IPN) electrolytes[26] have been investigated in the past two decades. Semi-IPN structure is composed of a cross-linked polymeric network and free polymer chains penetrated in the network.[27, 28] Semi-IPN electrolytes not only achieve the high ionic conductivity

via freely mobile lithium ion-conducting polymer segments, but also maintain the dimensional stability provided by the cross-linked network.[29] To prepare the cross-linked network structure in Semi-IPN electrolytes, flexible polymer chains have been generally used, including polysiloxane, low molecular weight PEO, and PMMA.[26, 30-32] Thus, the deterioration of mechanical properties is difficult to avoid when the Semi-IPN electrolytes contain a large amount of ion-conducting polymers.

Polyhedral oligomeric silsesquioxane (POSS) has attracted considerable interest as an effective nanofiller because of its well-defined nanoscale organic/inorganic hybrid structure.[33, 34] POSS has been known to improve mechanical strength of polymers due to the molecular level dispersion of rigid POSS moiety in the polymers,[35-37] while its significant volume can also maintain or decrease the glass transition temperature (T_g) by changing the polymer chain topology and providing additional free volume to the polymers.[38] In our recent studies, we reported that dimensionally-stable free-standing films can be obtained by incorporating POSS side groups into wax-state polymers with PEG side groups.[39, 40] T_gs of the

copolymers with both PEO and POSS side groups were found to be close to those of the homopolymers with only PEO side group. This indicates that the incorporation of POSS into polymers can improve the dimensional stability of polymers without significant decreases in polymer chain mobility. This effect of POSS on polymers promises the possibility of developing Semi-IPN electrolytes with enhanced ionic conductivity and dimensional stability by combining the Semi-IPN structure with POSS.

In this study, we demonstrate an approach to prepare organic/inorganic hybrid semi-IPN electrolytes (HIPEs) based on PEOEC, which can impart high ionic conductivity and sufficient dimensional stability for use in all-solid-state lithium batteries. Prior to investigating the HIPEs, the ionic conductivity behavior of PEOEC electrolyte is studied and compared with that of PEO electrolyte. The HIPEs are prepared by a photo-cross-linking reaction of octa-functional POSS acrylate (OA-POSS) and ethoxylated trimethylolpropane triacrylate (ETPTA) under the co-presence of PEOEC. The discussion mainly focuses on the effect of OA-POSS on solid-state electrolyte properties of the HIPEs, including

dimensional stability, thermal behavior, and ionic conductivity. Based on the understanding of the characteristics of HIPEs, the feasibility of applying the HIPEs to solid-state electrolytes for lithium batteries is attested by electrochemical stability and cell performance.

2. Experimental

2.1.Materials

Potassium hydroxide (KOH, Aldrich) was dried under high vacuum at 110 ^{o}C for 3 days and stored in an argon-filled glove box. Ethylene carbonate (EC, 98 %), poly(ethylene oxide) (PEO, GPC-MALLS analysis: M_w = 5,300 g mol^{-1}), trimethylopropane ethoxylate triacrylate (ETPTA, M_n = 428 g mol^{-1}), and 2-hydroxy-2-methyl-1-phenyl-1-propanone (HMPP), all from Aldrich, were used as received. Acrylo POSS® (OA-POSS, Product Number: MA0736) was purchased from Hybrid Plastics, Inc. and used as received. Lithium perchlorate ($LiClO_4$, > 99 %, Aldrich) and lithium trifluoromethanesulfonate ($LiSO_3CF_3$, 99.995 %,

Aldrich) were dried under high vacuum at 130 ^{o}C for 2 days and stored in an argon-filled glove box. Tetrahydrofuran (THF) was distilled from sodium/benzophenone under a nitrogen atmosphere. All other reagents and solvents were used as received from standard vendors.

2.2.Synthesis of poly(ethylene oxide-*co*-ethylene carbonate) (PEOEC).

Poly(ethylene oxide-*co*-ethylene carbonate) (PEOEC) was synthesized *via* ring opening polymerization of ethylene carbonate (EC). The following procedure was used for the preparation of high molecular weight PEOEC (H-PEOEC, GPC-MALLS analysis: M_w = 6,100 g mol^{-1}). EC (40 g, 0.45 mol) and potassium hydroxide (KOH, 0.13 g, 0.0023 mol) were added to a 100 mL round-bottomed flask equipped with a magnetic stirring bar in a glove box. Polymerization was conducted at 180 ^{o}C under nitrogen gas flow. After 2 h 30 min of polymerization, the flask was placed in liquid nitrogen and diluted with chloroform to quench the reaction. Then, chloroform was removed using a rotary evaporator. The polymer/monomer mixtures were dissolved in a small amount of ethanol and the solution was precipitated into an excess of diethyl ether to remove unreacted

monomers. The dissolution-precipitation procedure was repeated for several times. The purified polymer was dried under vacuum at room temperature for 3 days, yielding a yellowish wax (4.1 g). The lower molecular weight PEOEC (L-PEOEC, GPC-MALLS analysis: M_w = 5400 g mol^{-1}) was also prepared using the same procedure except the EC/KOH feed ratio (1000/1) and reaction time (2 h). ^1H NMR (300 MHz, $CDCl_3$, δ (ppm), tetramethylsilane (TMS) ref): 4.28 (CH_2-CH_2-O-C(O)-O), 3.72 (CH_2-CH_2-O-C(O)-O), 3.67 (CH_2-CH_2-O).

2.3.Preparation of polymer electrolytes based on PEO and PEOEC.

The polymers (PEO or (H- or L-)PEOEC) (0.2 g) and $LiClO_4$ in various blend compositions were dissolved homogeneously in distilled THF (0.8 ml). The concentration of lithium salt in polymer electrolytes is defined as the ratio of [Li (lithium salt)] / ([EO (ethylene oxide unit)] + [EC (ethylene carbonate unit)]). The solvent was evaporated using a rotary evaporator and further dried at 80 ^oC under high vacuum for a week. The PEO- and PEOEC-based polymer electrolytes were

designated as PEO# and (H- or L-)PEOEC#, where # is the lithium salt concentration in the electrolytes.

2.4.Preparation of organic/inorganic hybrid semi-interpenetrating network electrolytes (HIPEs).

Organic/inorganic hybrid semi-interpenetrating network electrolytes (H-HIPEs) containing H-PEOEC 0.15 and ETPTA/OA-POSS moieties were prepared by a solution casting and UV curing process. Polymers (H-PEOEC), cross-linkers (ETPTA and OA-POSS), photo-initiator (HMPP), and $LiClO_4$ were dissolved in distilled THF. The weight ratio of polymer : cross-linkers was fixed at 80 : 20, wherein the weight ratio of ETPTA : OA-POSS was 20 : 0, 15 : 5, and 10 : 10 for H-HIPE 0, H-HIPE 5, and H-HIPE 10, respectively. The injected mass of HMPP was 0.1 wt% of that of the crosslinkers. Organic/inorganic hybrid semi-interpenetrating network electrolytes (L-HIPEs) containing L-PEOEC 0.15 instead of H-PEOEC 0.15 were also prepared. The lithium salt concentration ([Li]

/ [EO] + [EC]) for the HIPEs was 0.15, at which the highest ionic conductivities of PEOEC electrolytes were observed. The homogeneous solution was casted on to a Teflon plate (2 × 2 cm^2) and the solvent was evaporated at room temperature for 12 h. Then, the casted mixture was exposed to UV light (B-100 series ultraviolet lamp, 50 Hz, UVP Inc., USA) for 10 min. The resultant film was dried at 80 ^oC under high vacuum for a week. The thickness of the HIPEs was in the range of 200–250 μm.

2.5.Electrochemical Analysis.

The ionic conductivities of the electrolytes were analyzed in a temperature range from 20 to 80 ^oC under a dry nitrogen condition using a ZAHNER IM-6ex impedance analyzer in the potentiostat mode with an AC amplitude of 10 mV over a frequency range from 100 mHz to 1 MHz. The PEO and PEOEC electrolytes were placed between two symmetrically aligned stainless steel electrodes in a Teflon cell with 200 μm spacers. The HIPE films were sandwiched by two

symmetrical stainless steel electrodes. The samples were thermally equilibrated at each temperature for 30 min prior to taking the measurements. The ionic conductivity, σ, was calculated using the equation, $\sigma = (1/R_b) \times (d/A)$, where R_b is the bulk electrolyte resistance, d is the thickness of the electrolytes, and A is the cross-sectional area of the electrode. The real part of the impedance at the minimum of the imaginary part was used as the resistance to calculate the conductivity of the electrolytes. The electrochemical stability was evaluated by linear sweep voltammetry (LSV) of an inert stainless steel electrode in HIPEs using a potentiostat (VMP3, Biologics) at 25 ^{o}C and 60 ^{o}C. The counter electrode was a Li metal foil. The cells for LSV measurements were assembled in an Ar-filled glove box (H_2O and O_2 < 0.1 ppm).

2.6.Galvanostatic Charge-Discharge Cycle Tests.

All-solid-state lithium cell of V_2O_5 / L-HIPE10 / Li metal was constructed, and its electrochemical characteristics were investigated. The cathode was prepared from

V_2O_5 (as a cathode active material), Super P (as an electronic conducting agent), and polyvinylidene fluoride (PVdF, as a binder) (60 : 20 : 20 in weight ratio) in N-methyl-2-pyrrolidone (NMP) solvents. The slurry was coated on an aluminium current collector using a doctor blade. The solvent was evaporated at 60 °C for 1 h and subsequently under high vacuum at 120 °C for 12 h. The thickness of the cathode layer was ca. 27 μm, and the mass of V_2O_5 in the cathode was ca. 0.85 mg cm^{-2}. L-HIPE10 (12 mg) was coated on the cathode (0.95 cm^2) via solution casting and UV curing process. The electrolyte-coated cathode was dried under high vacuum at 80 °C for 4 days. 2032 coin-type cells were assembled in an Ar-filled glove box (H_2O and O_2 < 0.1 ppm) as follows: The electrolyte-coated cathode was placed on the bottom of the cell, on which L-HIPE10 was placed, and the Li metal foil acting as the anode was placed on the electrolyte film; then the cell was sealed with stainless steel spacer and spring. After annealed at 60 ^oC for 12 h, the cells were galvanostatically charged and discharged in the voltage range from 2 to 4 V vs. Li/Li^+. The charge-discharge test was recorded at 25 μA cm^{-2} rate. All the electrochemical measurements were made with a WBCS3000 battery

cycler (WonATech) at 60 ^{o}C.

2.7.Characterization.

^{1}H NMR spectra were recorded on an Ascend^{TM} 400 spectrometer (300 MHz) using $CDCl_3$ (with a tetramethylsilane (TMS) reference) as the solvent at room temperature. Molecular weights (M_n, M_w) and polydispersity index (PDI) of PEO and PEOEC were analyzed by gel permeation chromatography (GPC). Relative molecular weights were measured by GPC equipped with a Waters 515 HPLC pump and three columns including PLgel 5.0 μm guard, MIXED-C, and MIXED-D from Polymer Laboratories in series with a Viscotek LR125 laser refractometer. The system with a refractive index (RI) detector was calibrated using polystyrene standards from Polymer Laboratories. The resulting data were analyzed using Omnisec software. GPC for the analysis of absolute molecular weights was performed using a Waters 515 HPLC pump equipped with three columns including PLgel 5.0 μm guard, MIXED-C, and MIXED-D from Polymer

Laboratories in series with a Wyatt Technology MiniDAWN^{TM} triple-angle light scattering detector (λ = 690.0 nm) and a Wyatt Technology Optilab DSP interferomeric refractometer. The data were processed using Wyatt's ASTRA V software. HPLC grade THF (J. T. Baker) was used as the eluent at a flow rate of 1.0 mL min^{-1} at 35 ^{o}C. The thermal transition behaviors of the polymers and electrolytes were examined by differential scanning calorimetry (DSC) using TA Instruments DSC-Q1000 under a nitrogen atmosphere. Samples with a typical mass of 3–7 mg were encapsulated in sealed aluminum pans. They were first heated to 150 ^{o}C and then quenched to –80 ^{o}C. This was followed by a second heating scan from –80 ^{o}C to 150 ^{o}C at a heating rate of 10 ^{o}C min^{-1}. The heat of fusion (ΔH_m) was calculated from the integral area between the baseline and each melting curve. The baseline was designated by connecting two points at which the instant value of its derivative curve becomes zero near the melting temperature (T_m). The thermal stability of HIPEs was investigated by thermogravimetric analysis (TGA) using TA Instruments TGA Q-5000IR under a nitrogen atmosphere. The samples were first heated to 130 ^{o}C and maintained at 130 ^{o}C for

10 min in order to evaporate residual water molecules, and then heated to 700 ^{o}C at a heating rate of 10 ^{o}C min^{-1}. Fourier transform infrared spectroscopy (FT-IR) of polymer electrolytes was performed on a Thermo Scientific Nicolet 6700 in the wavenumber range from 4000 to 400 cm^{-1} with a resolution of 4 cm^{-1} using KBr pellets. Temperature-resolved rheological measurement of HIPEs was carried out using a rheometer (Advansed Rheometric Expansion System, ARES) in the linear viscoelastic region with 0.1 rad s^{-1} of frequency at 1 ^{o}C min^{-1} ramp.

3. Result and Discussion

3.1.Synthesis of Poly(ethylene oxide-co-ethylene carbonate).

Poly(ethylene oxide-*co*-ethylene carbonate) (PEOEC) was synthesized via ring opening polymerization of ethylene carbonate (EC) using potassium hydroxide as an initiator (Scheme 1). In order to investigate the effect of molecular weight on the properties of PEOEC-based electrolytes, higher and lower molecular weight

PEOECs were prepared; $M_{w,\,MALLS}$ = 6,100 g mol^{-1} and $M_{w,\,MALLS}$ = 4,500 g mol^{-1} for H-PEOEC and L-PEOEC, respectively (Table 1). The molecular weight of PEOEC could be controlled by EC/KOH feed ratio and reaction time as described in the Experimental section.[17] Figure 1(b) shows the ^{1}H NMR spectrum with the assignments of the respective peaks of PEOEC. The proton peaks observed at 3.72 and 4.28 ppm were clearly assigned to EC units in PEOEC. In addition, a proton peak at 3.65 ppm indicates the presence of ethylene oxide (EO) units in the polymers. Aside from the EC repeating unit, EO repeating unit is formed during the polymerization due to the evolution of CO_2 gas.[17] The proton peak from ethylene carbonate monomer (δ= 4.54 ppm) was not observed in the polymer, suggesting that the unreacted monomer was successfully removed during the precipitation. The content of EC unit in PEOECs was calculated from the ^{1}H NMR data as follows:

$$\text{EC Content (mol \%)} = (I_{b+c}/\, I_{a+b+c}) \times 100 \qquad (1)$$

Where I_a, I_b, and I_c are the integrated intensities of a, b, and c proton peaks in Figure 1(b), respectively. As shown in Table 1, the EC contents of L-PEOEC and H-PEOEC are close; 33 and 31 mol % for L-PEOEC and H-PEOEC, respectively. In our previous work, EC-EO-EO repeating unit was found to be the major structural unit in the PEOEC, which can be formed by the combination of two alkylene carbon attacks and one carbonyl carbon attack by the active chain end (Figure S1).[17] Therefore, the EC contents in PEOECs (31–33 mol %) are reasonable.

For comparison purposes, poly(ethylene oxide) (PEO) was obtained from a commercial source and characterized (Table 1). The PEO in this study exhibits a solid state at room temperature due to its semi-crystalline structure (Figure S2). Although the molecular weight of H-PEOEC ($M_{w,\ MALLS}$ = 6,100 g mol^{-1}) is slightly larger than that of PEO ($M_{w,\ MALLS}$ = 5,300 g mol^{-1}), H-PEOEC was found to be in wax state due to the presence of EC units in the polymers. The formation of crystalline domains of PEO segments in PEOEC should be disturbed by the randomly distributed EC units. In comparison to PEO, no melting transition peak

was observed in PEOEC from DSC analysis (Figure S2), indicating that PEOEC is an amorphous polymer without any crystalline phase.

Scheme 1. Synthesis of poly(ethylene oxide-*co*-ethylene carbonate) (PEOEC).

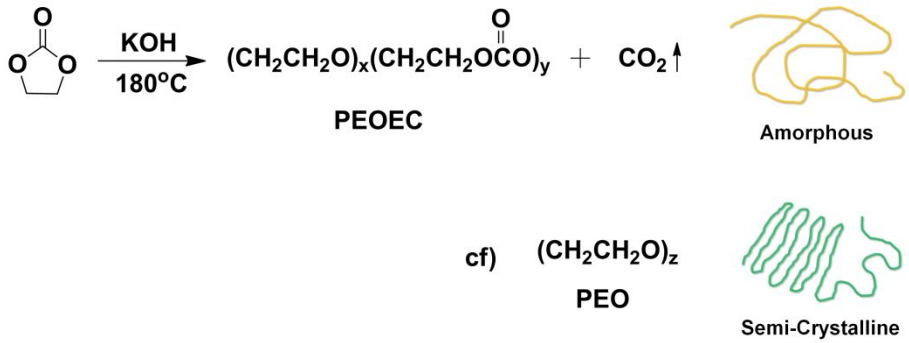

Table 1. Composition, Molecular Weight, PDI, and State of Poly(ethylene oxide-*co*-ethylene carbonate) (PEOEC) and Poly(ethylene oxide) (PEO).

Sample	Composition [a] (EO : EC) [mol%]	M_w [b] [RI]	M_w [c] [MALLS]	PDI [b(c)]	State [d]
L-PEOEC	67 : 33	4,800	4,900	1.67 (1.35)	Wax
H-PEOEC	69 : 31	6,700	6,100	1.61 (1.15)	Wax
PEO	100 : 0	6,300	5,300	1.06 (1.02)	Solid

[a] Obtained by ^{1}H NMR. [b] Determined by GPC using refractive index (RI) detector (THF), calibrated with linear polystyrene standard. [c] Determined by GPC using multi-angle laser light scattering (MALLS) detector (THF). [f] After casted on Teflon plate from THF solution and dried at room temperature.

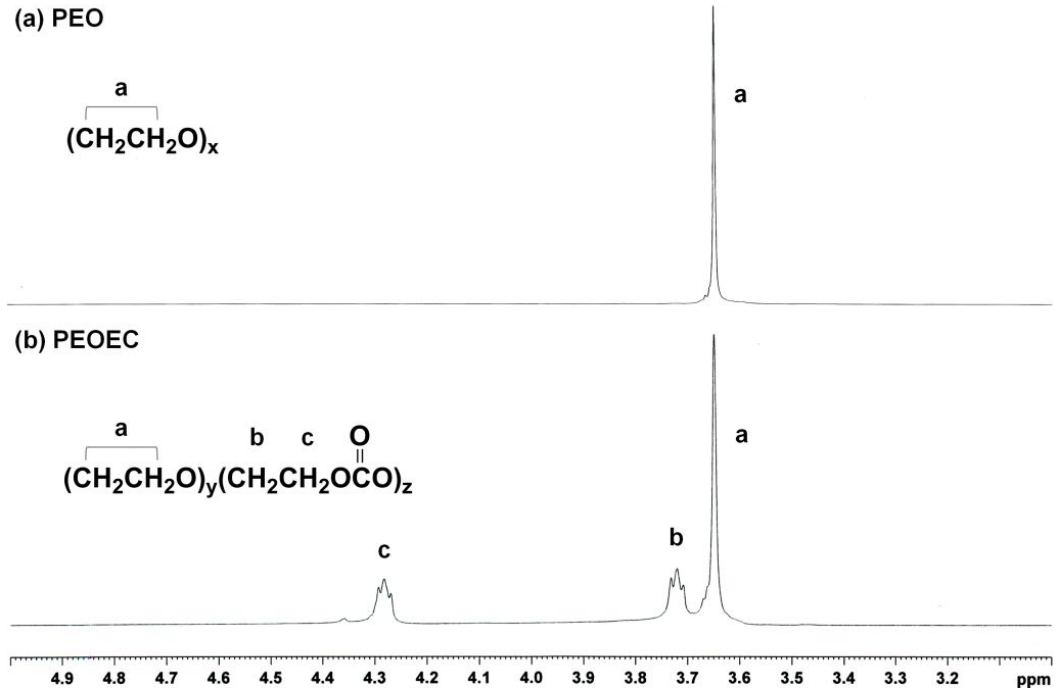

Figure 1. ^{1}H NMR Spectra of (a) PEO and (b) PEOEC.

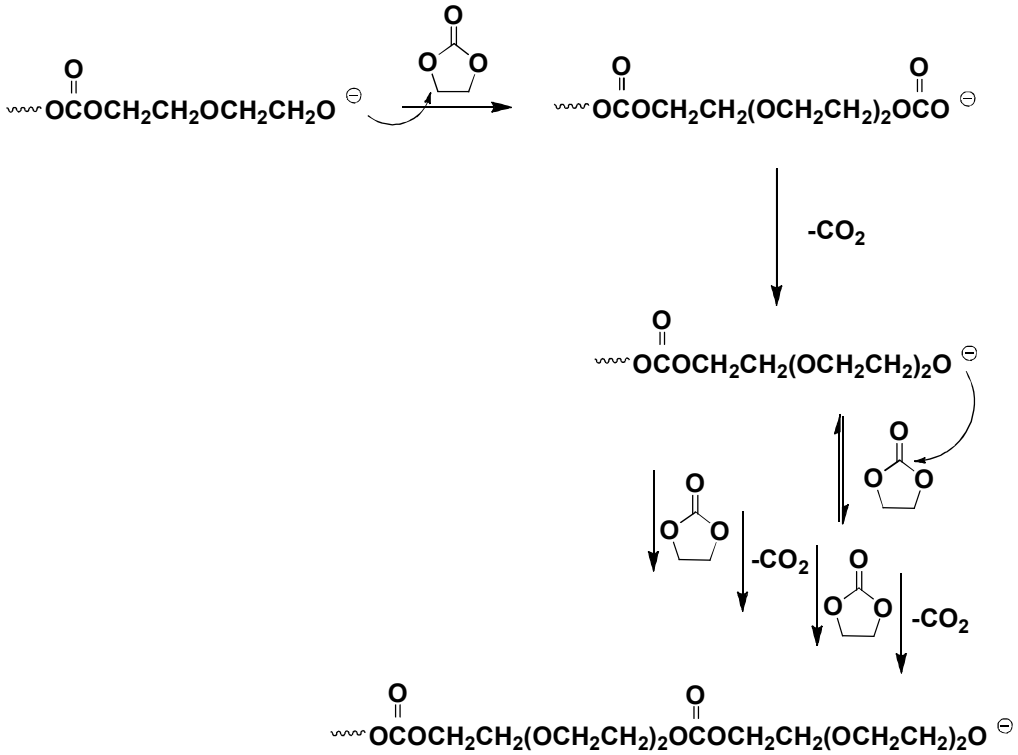

Figure S1. Mechanism of Formation of the Major Repeating Unit (EC-EO-EO) in PEOEC.

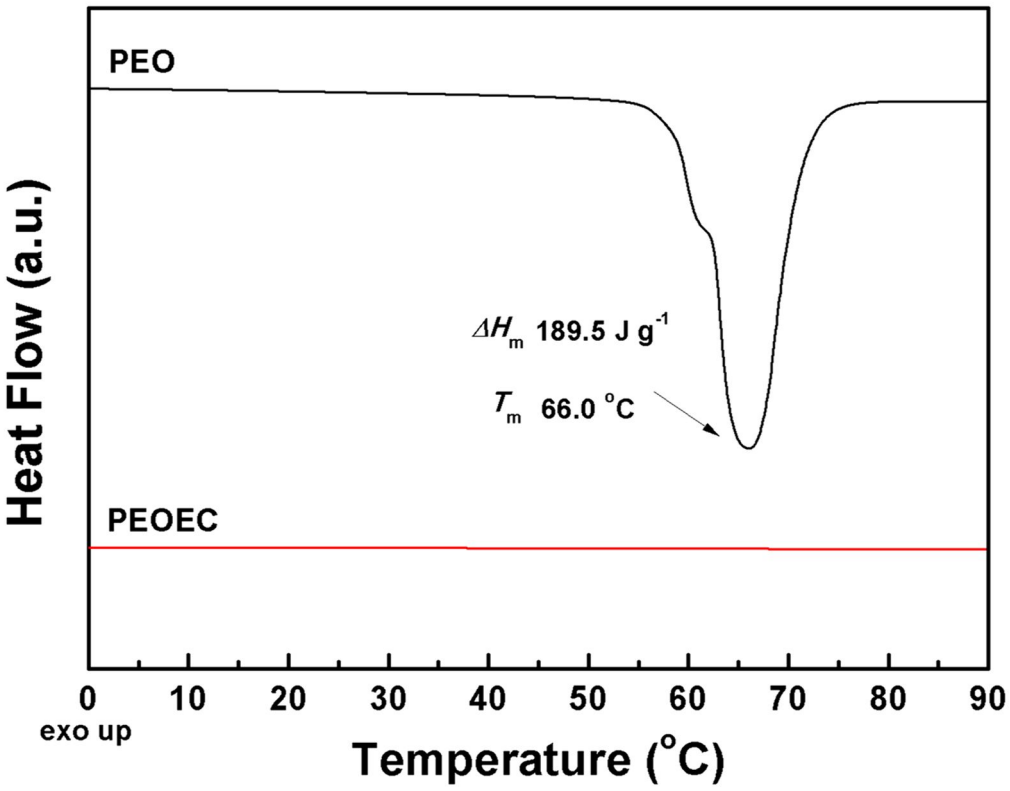

Figure S2. DSC Curves of PEO and PEOEC without lithium salt.

3.2.Effect of ethylene carbonate unit on ionic conductivity of PEOEC electrolytes.

Prior to investigating the properties of organic/inorganic hybrid semi-interpenetrating network electrolytes (HIPEs), the ionic conductivity behaviors of PEOEC electrolytes were studied in detail. The ionic conductivities of PEO and H-PEOEC electrolytes with various $LiClO_4$ concentrations at 30 ^oC were measured to investigate the effect of lithium salt concentration and ethylene carbonate unit in the polymer electrolytes on the ionic conductivity (Figure 2). Maximum ionic conductivity of PEO electrolytes was observed at a [Li]/([EO]+[EC]) ratio of 0.09. The ionic conductivity is related to the number of charge carriersand their mobility as follows:

$$\sigma = \Sigma\, n \times q \times \mu$$

where n is the number of charge carriers, q is the charge on the charge carrier,

and μ is the mobility of the charge carrier.[41] Therefore, when the salt concentration ([Li]/([EO]+[EC])) is smaller than 0.09, the increase in conductivity is ascribed to the increase in the number of lithium ions. The subsequent decrease in ionic conductivity, when the salt concentration is larger than 0.09, can be explained by the decrease in the chain mobility of PEO segments. The T_g values of PEO increase with increasing lithium salt concentration as shown in Figure 3. The lithium salt in PEO restricts the segmental motion of the polymer matrix by intra- and/or inter-molecular coordination with the oxygen in the PEO.[25, 42]

The ion-ion interaction in the electrolytes with $LiClO_4$ was studied by FT-IR analysis. In Figure S3, one band observed at 623 cm^{-1} is assigned to ClO_4^- dissociated ion vibration, and the other one observed at 633 cm^{-1} is assigned to the vibration of $Li^+ClO_4^-$ contact ion pairs.[43] The fraction of dissociated ions and contact ion pairs can be calculated by integrating the area under the two peaks. As shown in Figure 4(a), when the salt concentration increases, the number of dissociated ions in the PEO electrolytes increases until the salt concentration reaches at 0.09 and became saturated. It indicates that the number of contact ion

pairs or aggregated ion increases after the salt concentration 0.09.[44] Thus, the decrease of effective charge carrier fractions for ionic charge transport should also contribute to the decrease in ionic conductivity at a larger salt concentration. This ionic conductivity behavior for PEO electrolytes was also observed for H-PEOEC electrolytes.

The maximum ionic conductivity of H-PEOEC electrolytes observed at a [Li]/([EO]+[EC]) ratio of 0.15 was 4.48×10^{-5}S cm^{-1}. The value is about four times of magnitude larger than that of PEO electrolytes (1.21×10^{-5} S cm^{-1}). As the molecular weight of H-PEOEC is even larger than that of PEO in this study (Table 1), the higher ionic conductivity of H-PEOEC electrolytes compared to that of the PEO electrolytes should not be the effect of the molecular weight. This should be affected by two factors. One is the higher mobility of H-PEOEC than PEO. H-PEOEC electrolytes were found to be completely amorphous without any crystalline phase due to the randomly distributed EC units in the polymers (Figure 3). The PEO electrolyte with a [Li]/([EO]+[EC]) ratio of 0.09 shows T_m peak at around 43 ^{o}C, indicating the presence of crystalline domains in the electrolytes.

Although the PEO electrolytes have lower T_g than the H-PEOEC electrolytes, the crystalline domains in the PEO electrolytes should interfere with lithium ion conduction, resulting in the lower ionic conductivity.[9]

The other is the larger content of dissociated lithium ions in PEOEC electrolytes than in PEO electrolytes. . It is well-known that the increase in dielectric constant of electrolytes increases the dissociation of lithium salts.[16] The number of dissociated ions in 1g of H-PEOEC electrolyte (9.8×10^{20}) is larger than that of PEO electrolyte (9.5×10^{20}), when they have the same salt concentration ([Li]/([EO]+[EC]) = 0.09). Furthermore, the maximum number of dissociated ions in 1g of H-PEOEC electrolytes was observed at a larger concentration ([Li]/([EO]+[EC]) = 0.15), whereas the maximum fraction of dissociated ions of PEO electrolytes was observed at a smaller concentration ([Li]/([EO]+[EC]) = 0.09). This should be ascribed to the existence of polar EC units in PEOEC. Since the polar EC moiety has higher dielectric constant than EO moiety,[15, 16] the more favorable dissociation of lithium salts in PEOEC than in PEO is expected. The interactions between EC units in PEOEC and lithium ions

were also confirmed by FT-IR. As shown in Figure S4, when the lithium salt was added to PEOEC, the EC band at 1743 cm^{-1} was found to shift to slightly higher wave numbers and a shoulder peak appeared at 1725 cm^{-1}, indicating the interaction between EC moieties and lithium ions.[20] As the ionic conductivity is proportional to the number of charge carriers as well as the mobility of charge carriers (eq. 2), these two factors improved by EC units in PEOEC led to the increase in ionic conductivity of PEOEC electrolytes compared to that of PEO electrolytes. In addition, the H-PEOEC electrolytes exhibit higher ionic conductivity than the PEO electrolytes even at temperatures above the T_m of PEO electrolytes (Figure S5), although the T_gs of H-PEOEC electrolytes are higher than those of PEO electrolytes. The higher ionic conductivity of H-PEOEC electrolytes than PEO electrolytes at the elevated temperature should be ascribed to the larger amount of dissociated lithium ions in the electrolytes (Figure 4).

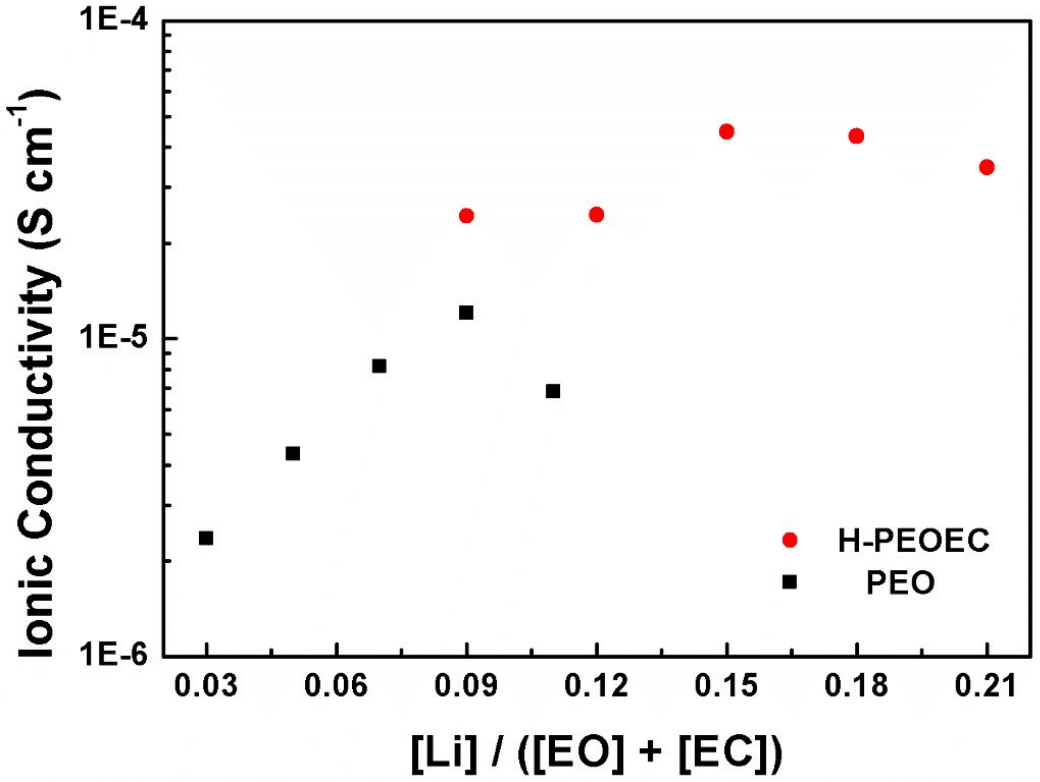

Figure 2. Ionic Conductivities of PEO and H-PEOEC Electrolytes with Various $LiClO_4$ Concentrations at 30°C.

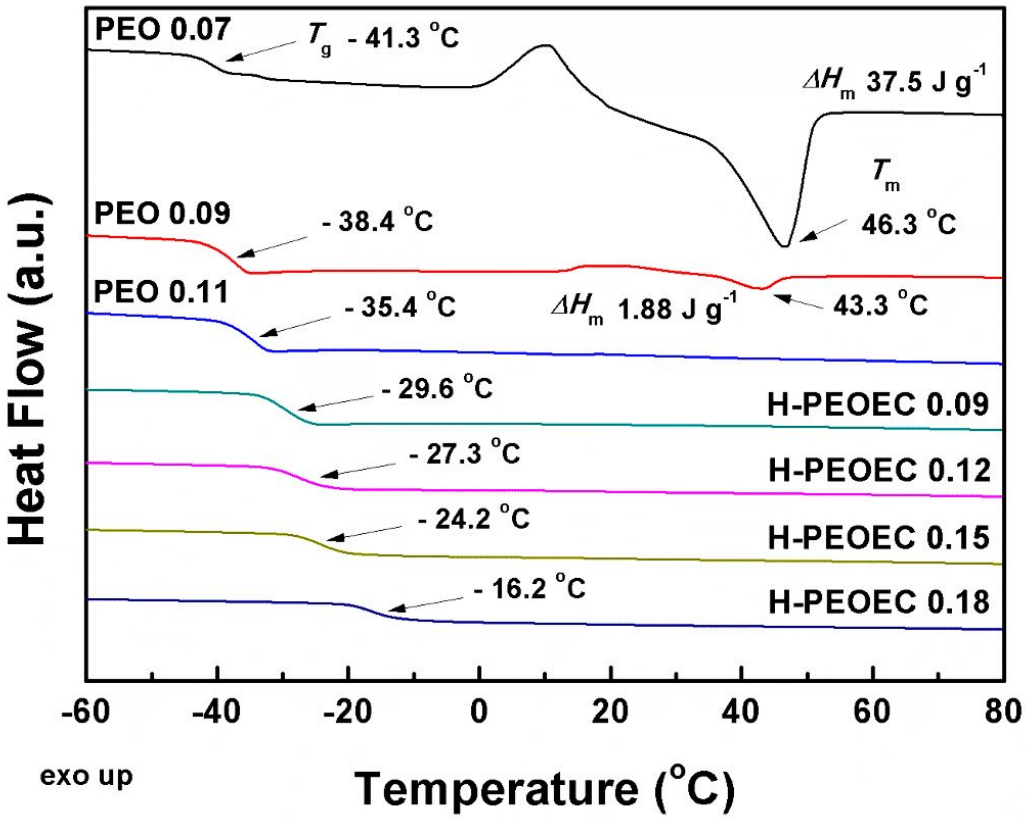

Figure 3. DSC Curves of PEO and H-PEOEC with Various $LiClO_4$ Concentrations.

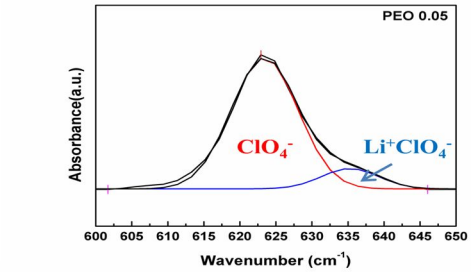
PEO 0.05
Absorbance(a.u.)
ClO_4^-
$Li^+ClO_4^-$
600 605 610 615 620 625 630 635 640 645 650
Wavenumber (cm^{-1})

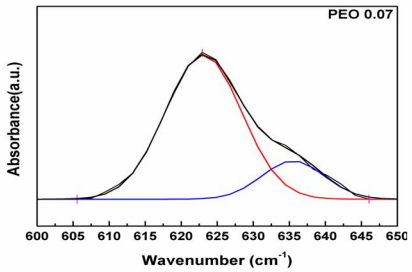
PEO 0.07
Absorbance(a.u.)
600 605 610 615 620 625 630 635 640 645 650
Wavenumber (cm^{-1})

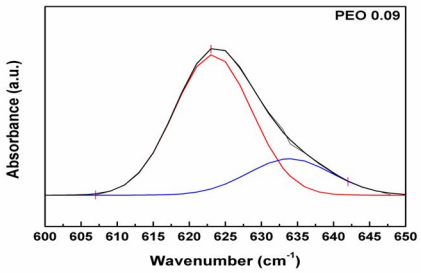
PEO 0.09
Absorbance (a.u.)
600 605 610 615 620 625 630 635 640 645 650
Wavenumber (cm^{-1})

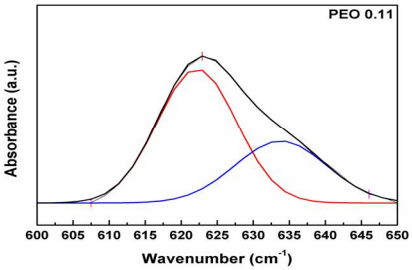
PEO 0.11
Absorbance (a.u.)
600 605 610 615 620 625 630 635 640 645 650
Wavenumber (cm^{-1})

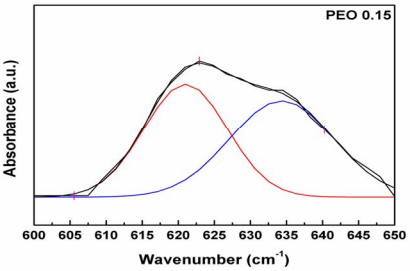
PEO 0.15
Absorbance (a.u.)
600 605 610 615 620 625 630 635 640 645 650
Wavenumber (cm^{-1})

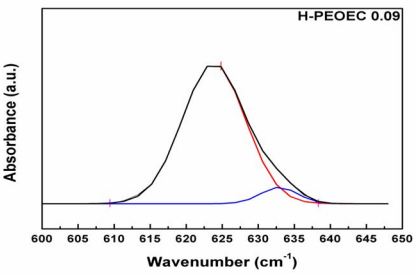
H-PEOEC 0.09
Absorbance (a.u.)
600 605 610 615 620 625 630 635 640 645 650
Wavenumber (cm^{-1})

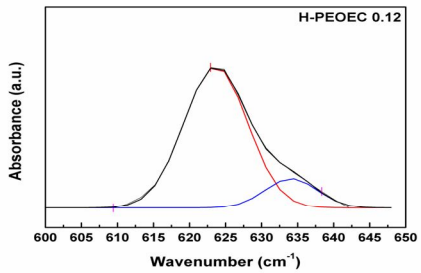
H-PEOEC 0.12
Absorbance (a.u.)
600 605 610 615 620 625 630 635 640 645 650
Wavenumber (cm^{-1})

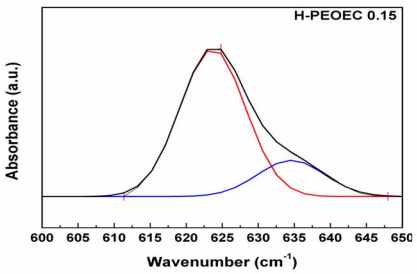
H-PEOEC 0.15
Absorbance (a.u.)
600 605 610 615 620 625 630 635 640 645 650
Wavenumber (cm^{-1})

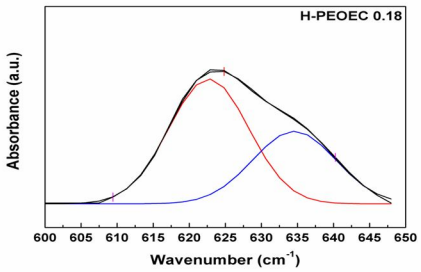
H-PEOEC 0.18
Absorbance (a.u.)
600 605 610 615 620 625 630 635 640 645 650
Wavenumber (cm^{-1})

Figure S3. FT-IR Spectra of PEO and H-PEOEC with Various $LiClO_4$ Concentrations in the Region of 600-650 cm^{-1}.

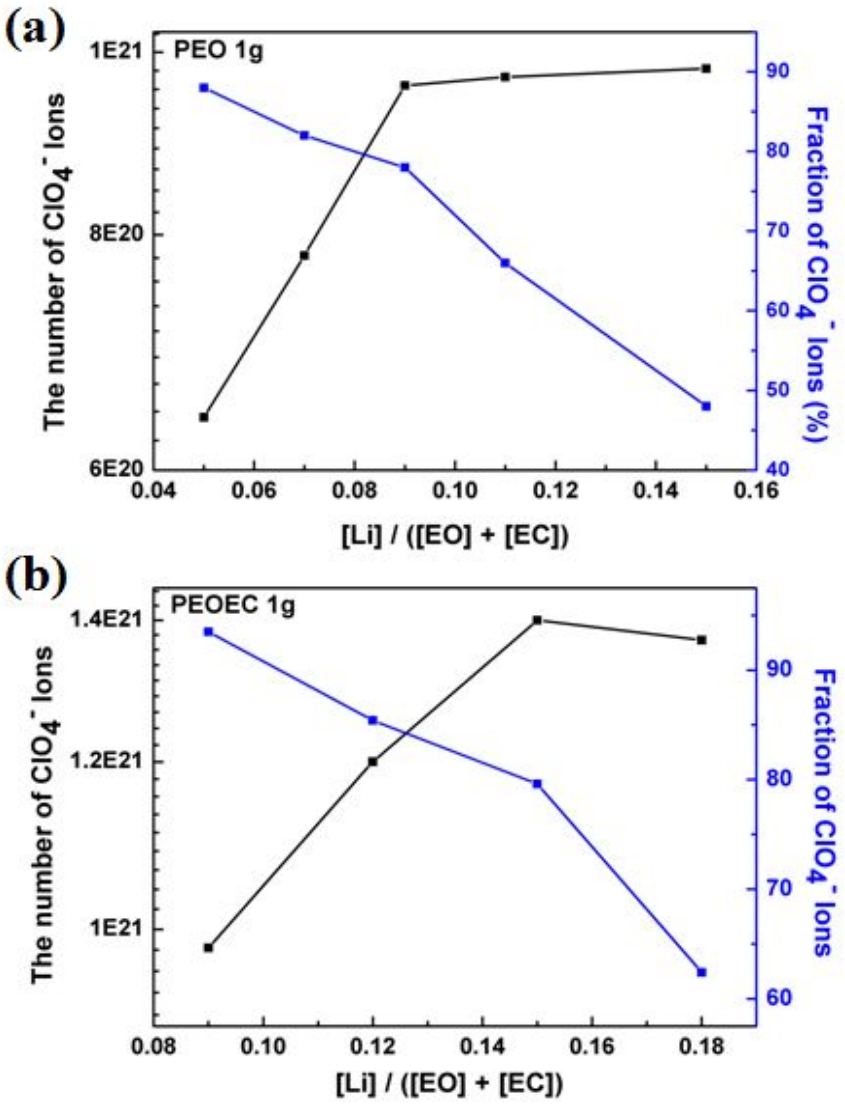

Figure 4. The Number and Fraction of Dissociated (ClO_4^-) ($Li^+ClO_4^-$) Ions Based on FT-IR Analysis of (a) PEO and (b) H-PEOEC with various $LiClO_4$ Concentrations

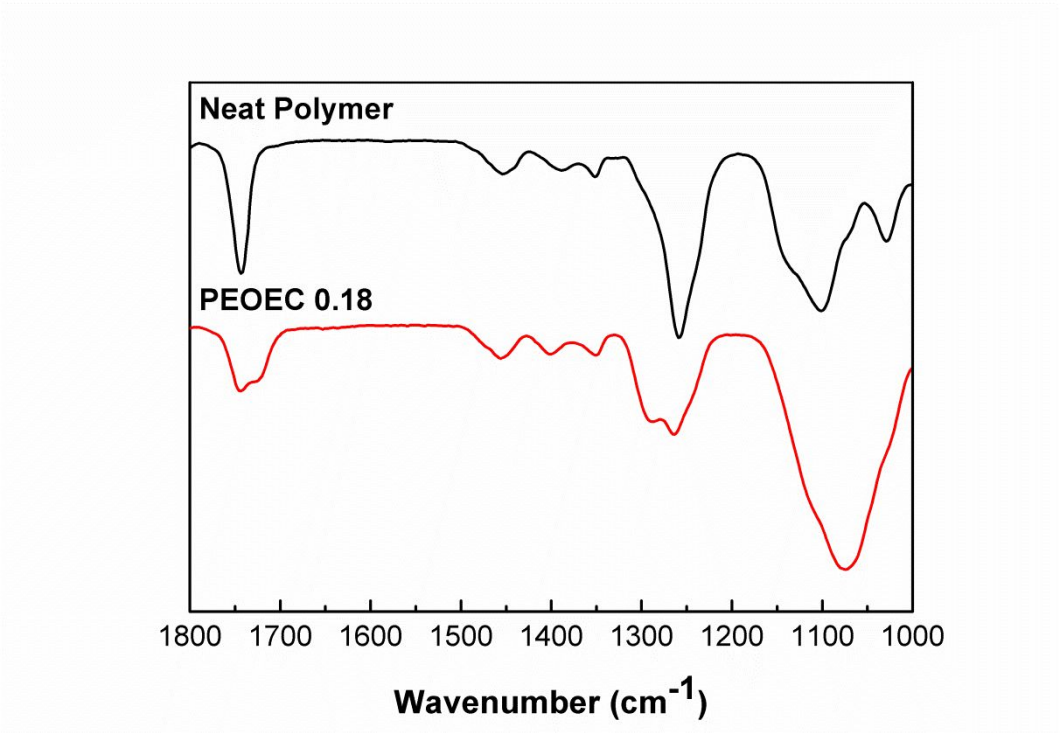

Figure S4. FT-IR Spectra of H-PEOEC with and without $LiClO_4$.

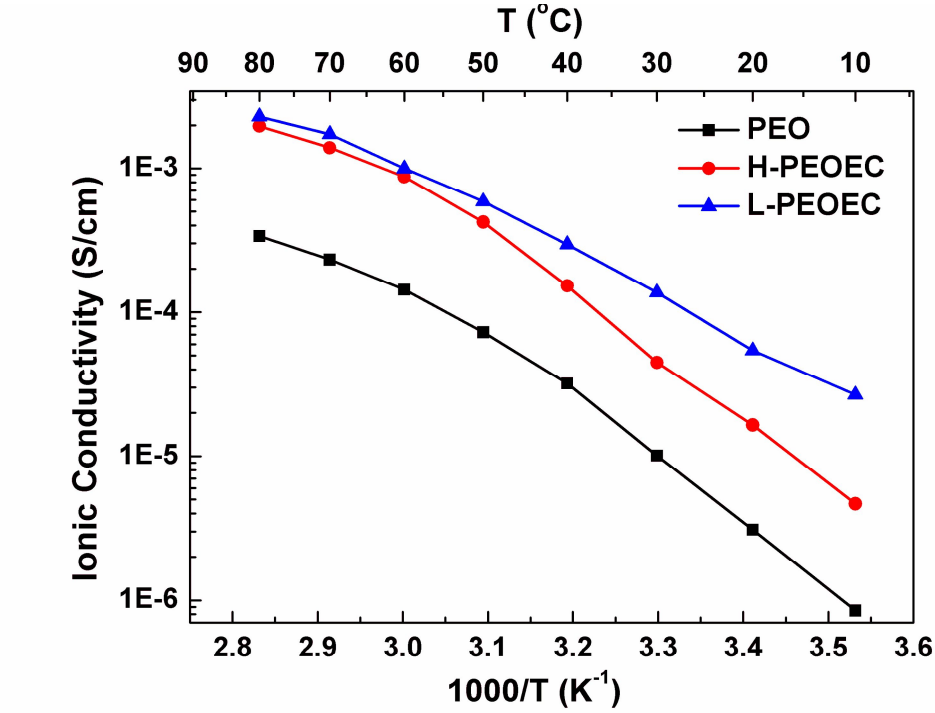

Figure S5. Temperature dependence of ionic conductivity of PEO ([Li] / ([EO] + [EC]) = 0.09) and (H-/L-)PEOEC electolytes ([Li] / ([EO] + [EC]) = 0.15) with $LiClO_4$.

3.3.Effect of molecular weight of PEOEC on Ionic Conductivity.

Figure 5 shows the ionic conductivities of H-PEOEC and L-PEOEC electrolytes with various lithium salt concentrations at 30°C. Although ionic conductivities of L-PEOEC electrolytes are always higher than those of H-PEOEC electrolytes, both electrolytes exhibit similar ionic conductivity behaviors. The maximum ionic conductivities for both electrolytes were observed at the same salt concentration ([Li] / [EO] + [EC] = 0.15) possibly due to the similar EC contents in the polymers; the values are 4.48×10^{-5} and $1.36 \times 10^{-}4$ S cm^{-1} for H-PEOEC and L-PEOEC electrolytes, respectively. The L-PEOEC electrolytes were found to have the saturated number of dissociated ions at a [Li]/([EO]+[EC]) ratio of 0.15, as do the H-PEOEC electrolytes (Figure 4(b) and Figure S6).The higher ionic conductivities of L-PEOEC electrolytes than those of H-PEOEC electrolytes should be attributed to the larger chain mobility as expected by the smaller T_g values (Figure 3 and Figure S7), which originates from the lower molecular weight of L-PEOEC than H-PEOEC.

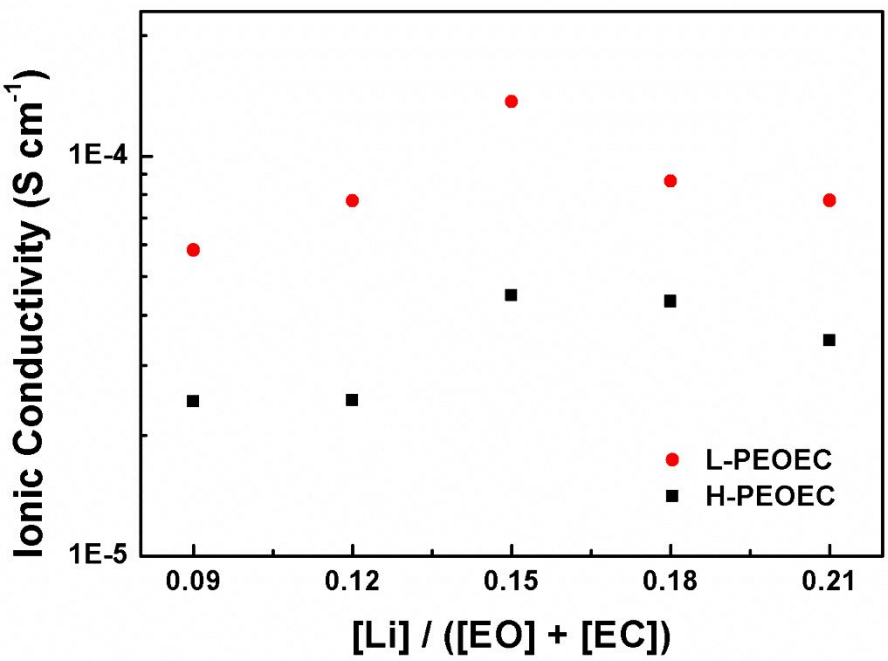

Figure 5. Ionic Conductivities of L-PEOEC and H-PEOEC Electrolytes with Various $LiClO_4$ Concentrations at 30°C.

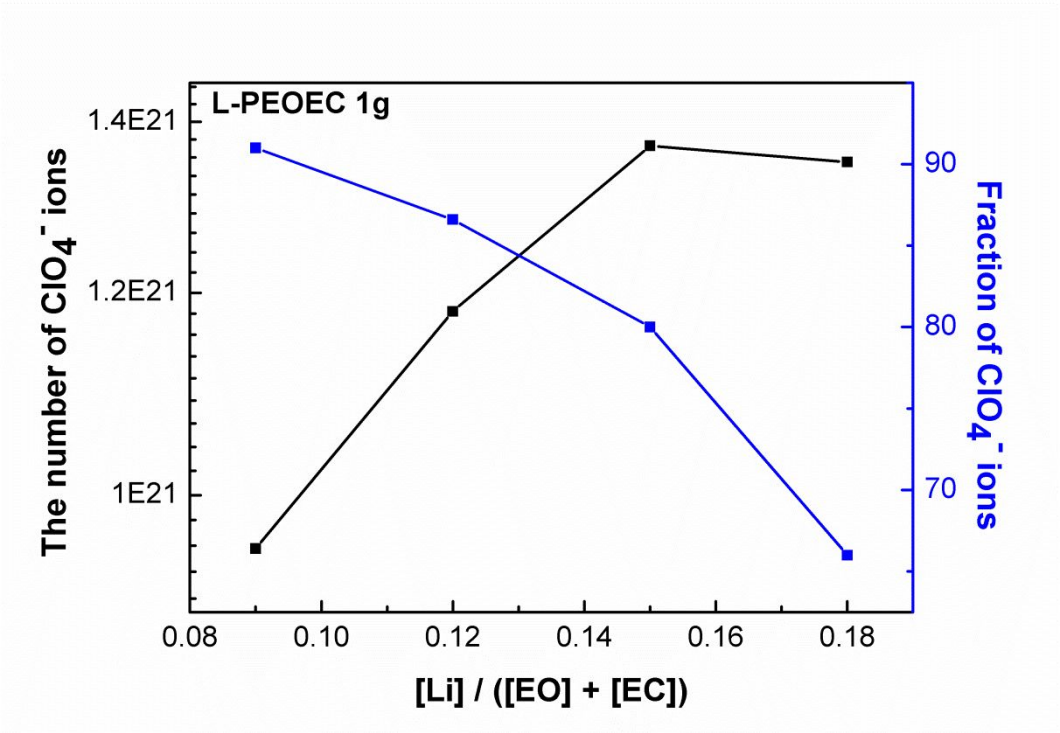

Figure S6. The number and Fraction of Dissociated (ClO_4^-) Ions Based on FT-IR Analysis of L-PEOEC with various $LiClO_4$ Concentrations.

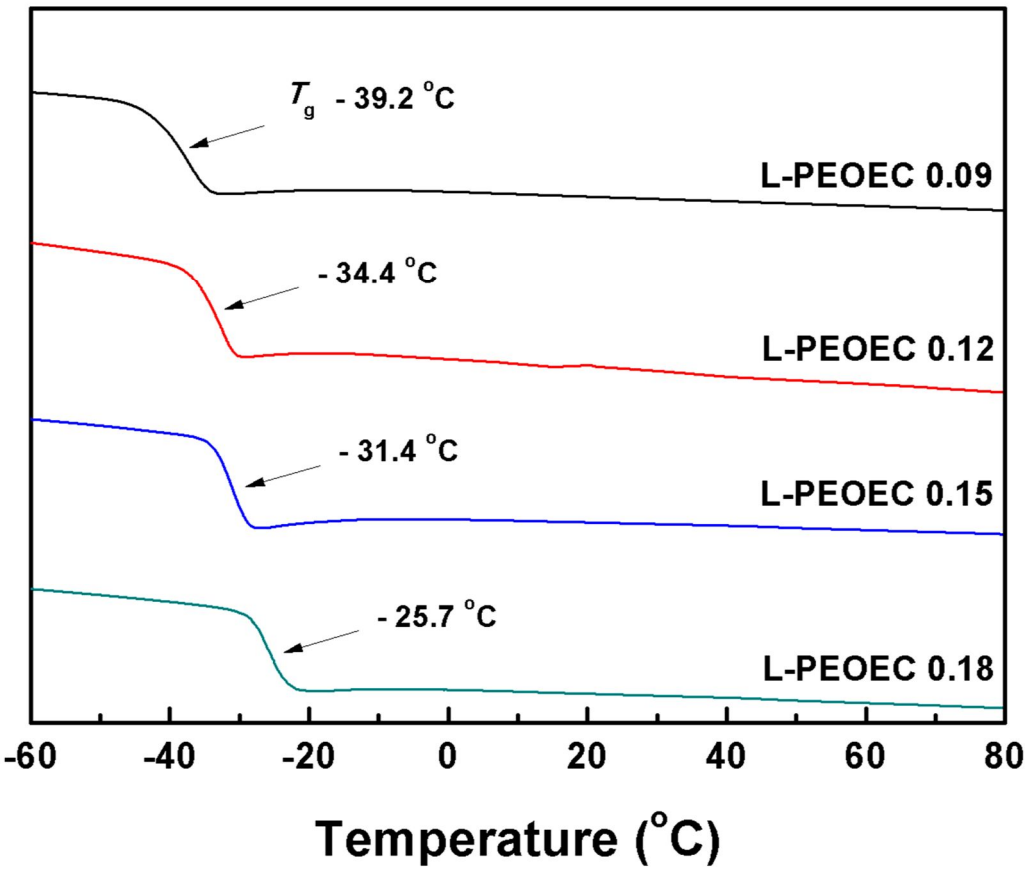

Figure S7. DSC Curves of L-PEOEC with various $LiClO_4$ Concentrations.

3.4.Preparation of Organic/Inorganic Hybrid Semi-interpenetrating Network Electrolytes (HIPEs).

Although the PEOEC electrolytes exhibit high ionic conductivities over 10^{-4} S cm^{-1} at 30 ^{o}C, they cannot be directly applied to all-solid-state lithium batteries due to their waxy nature. Thus, based on the understanding of unique ionic conductivity behavior of PEOEC electrolytes, we studied the architecture and solid-state electrolyte properties of HIPEs containing PEOECs. A schematic illustration for the preparation of HIPEs is described in Scheme 2. A series of HIPEs consisting of different contents of PEOEC electrolytes ([Li]/([EO]+[EC]) = 0.15) as a lithium ion conductor and ETPTA/OA-POSS moieties as organic/inorganic hybrid network structure were prepared by solution casting and UV curing process (Table 2). The UV curing reaction of HIPEs was examined by FT-IR (Figure S8). The peaks from acrylic C=C bonds of ETPTA and OA-POSS at 1610–1625 cm^{-1} were not observed for HIPEs after 10 min of UV irradiation, demonstrating the completion of photo-cross-linking reaction of ETPTA/OA-POSS cross-linkers.

The HIPEs are designated as H- or L-HIPE#, where H and L indicate the presence of H-PEOEC and L-PEOEC in HIPEs, respectively, and # is the weight percentage of OA-POSS in the HIPEs. Flexible free-standing films could be obtained when the total content of ETPTA and OA-POSS was larger than 20 wt % (Scheme 2), while when the content of cross-linkers was smaller than 15 wt %, the HIPEs became sticky and flimsy. Thus, the weight ratio of PEOEC : cross-linkers was fixed at 80 : 20. In order to investigate the effect of OA-POSS on the dimensional stability, thermal behavior, and ionic conductivity of HIPEs, we prepared HIPEs with OA-POSS content of 0, 5, and 10 wt% for HIPE0, HIPE5, and HIPE10, respectively. We also tried to make HIPEs with OA-POSS content larger than 15 wt % using the same procedure. However, we could not obtain homogeneous, free-standing films from the compositions, possibly due to the incompatibility of a large amount of hydrophobic OA-POSS with hydrophilic PEOEC polymers (Figure S9). As the PEOEC electrolytes exhibit the maximum ionic conductivities at a [Li]/([EO]+[EC]) ratio of 0.15 (Figure 5), the salt concentration of 0.15 was used for all the HIPEs.

Scheme 2. Preparation of Organic/Inorganic Hybrid Semi-Interpenetrating Network Electrolytes Based on PEOECs (HIPEs).

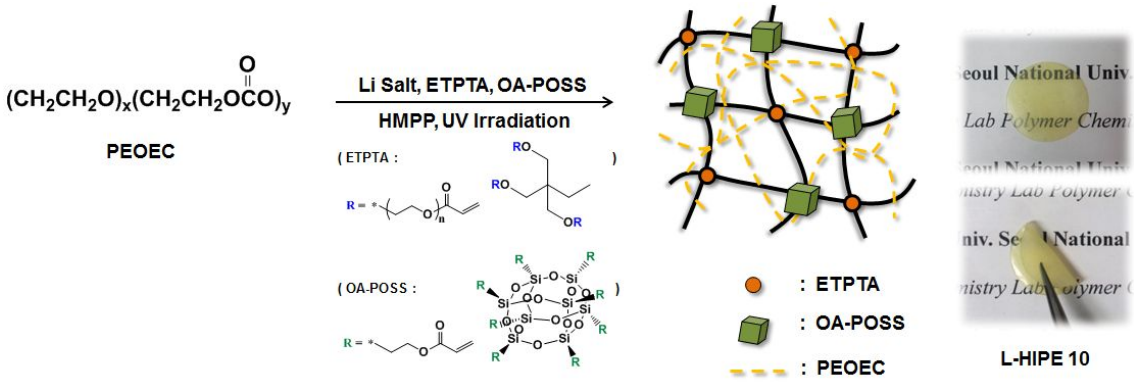

Table 2. Composition and Thermal Properties of HIPEs.

Sample [a]	Composition (PEOEC : ETPTA : POSS) [wt%]	$T_{d,\,5\%}$ [d] (^{o}C)	T_{g} [e] (^{o}C)
H-HIPE 0 [b]	80 : 20 : 0	245	-3.9
H-HIPE 5 [b]	80 : 15 : 5	250	-6.1
H-HIPE 10 [b]	80 : 10 : 10	266	-8.5
L-HIPE 0 [c]	80 : 20 : 0	223	-9.9
L-HIPE 5 [c]	80 : 15 : 5	232	-14.8
L-HIPE 10 [c]	80 : 10 : 10	237	-17.1

[a] Samples with $LiClO_4$ ([Li] / [EO] + [EC] = 0.15). [b] H-PEOEC ($M_{w,\,MALLS}$: 6,100) is used. [c] L-PEOEC ($M_{w,\,MALLS}$: 4,800) is used. [d] The decomposition temperature, $T_{d,\,5\%}$, is defined as 5 wt% loss. [e] Obtained by DSC equipped with RCS at a heating rate of 10 ^{o}C/min.

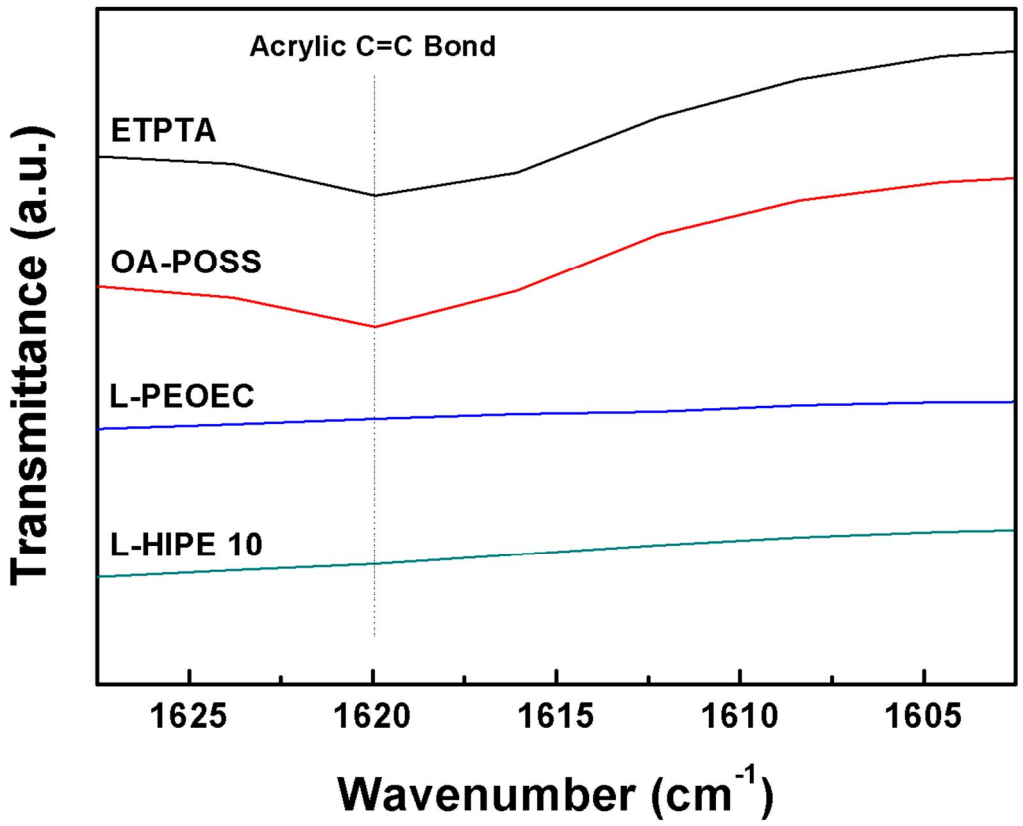

Figure S8. FT-IR Spectra of ETPTA, OA-POSS, L-PEOEC, and L-HIPE 10.

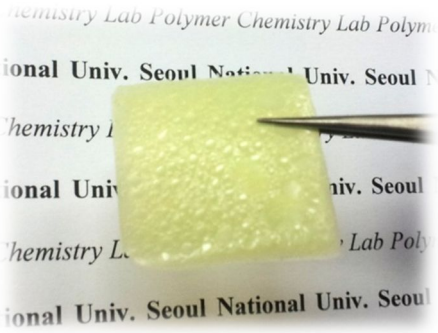

Figure S9. Photographs of L-HIPE15 with 80 wt% L-PEOEC / 5 wt% ETPTA / 15 wt% OA-POSS.

3.5.Dimensional Stability of HIPEs.

Dimensional stability of HIPEs was investigated by temperature-resolved rheological measurements as shown in Figure 6. Solid-like behaviors of HIPEs were observed over the range of temperatures (30–80 ^{o}C), as indicated by the larger dynamic storage modulus (*G'*) than dynamic loss modulus (*G"*).[45] In addition, the *G'* values were found to remain stable for all the HIPEs. These results suggest that dimensionally-stable free-standing electrolyte films can be prepared by utilizing the organic/inorganic hybrid semi-interpenetrating network structures. The *G'* values of HIPEs increase with increasing OA-POSS content, indicating that HIPEs with larger OA-POSS content have higher dimensional stability than HIPEs with smaller OA-POSS content. The increase in *G'* values of HIPEs should not be the effect of cross-linking density, because the molar content of acrylic C=C bond moieties decreases in HIPEs with increasing OA-POSS content.[46, 47] This should be attributed to the increase of POSS content in HIPEs. It has been reported by others that the introduction of rigid POSS moieties into

polymeric matrix increased the *G'* values, which originates from the reinforcement effect of POSS.[45, 48] Meanwhile, the storage modulus of L-HIPE10 was found to be smaller than that of H-HIPE10 due to the lower molecular weight PEOEC in L-HIPEs than in H-HIPEs (Figure S10).[49, 50] However, the L-HIPE10 still maintains a stable free-standing film state with a large storage modulus of ~ 10^5 Pa, which is sufficient dimensional stability for a SPE application in lithium batteries.[51] The details of fabrication and characterization of all-solid-state lithium batteries with L-HIPE10 are discussed in the later part of this article.

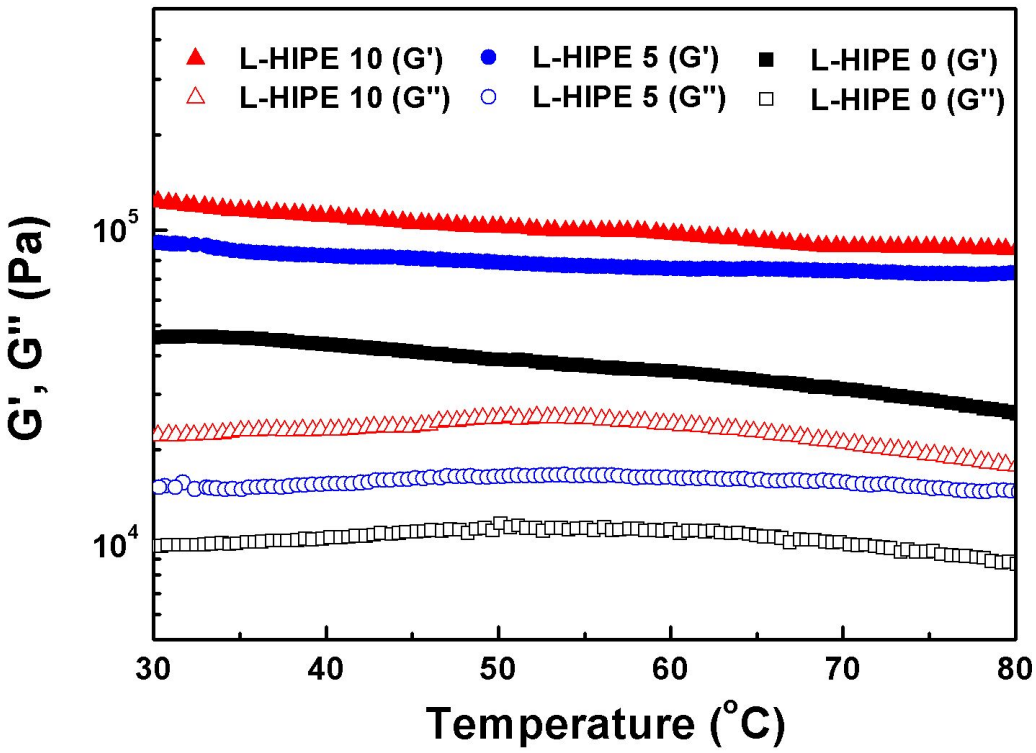

Figure 6. Temperature-Resolved Rheological Behaviors of L-HIPEs in the Linear Viscoelastic Region with 1 rad s^{-1} of Frequency at 1 ^{o}C min^{-1} Ramp.

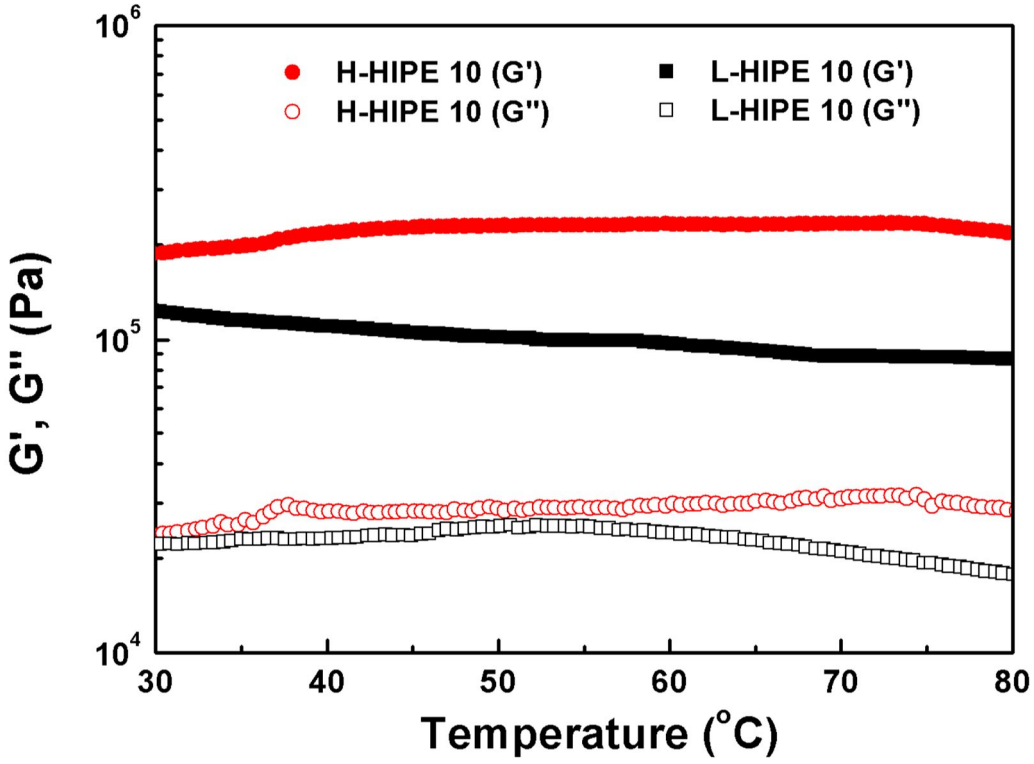

Figure S10. Temperature-Resolved Rheological Behaviors of H-HIPE10 and L-HIPE10 in the Linear Viscoelastic Region with 1 rad s^{-1} of Frequency at 1 ^{o}C min^{-1} Ramp.

3.6.Thermal Properties of HIPEs.

Thermal stability of HIPEs was examined by TGA. The thermal decomposition temperatures at 5 % weight loss ($T_{d,5\%}$) of the samples are listed in Table 2. The $T_{d,5\%}$ values of H-HIPEs are larger than those of L-HIPEs, possibly due to the higher molecular weight PEOEC in H-HIPEs than in L-HIPEs.[52] Both H-HIPEs and L-HIPEs exhibit higher thermal stability when they have larger OA-POSS content. Since the molar content of acrylic C=C bond moieties in HIPEs is even smaller when they have larger OA-POSS content, the increased $T_{d,5\%}$ values should have resulted from the thermally stable POSS structure in OA-POSS cross-linker. The increase in thermal stability of polymeric matrix induced by the incorporation of POSS moieties into the polymer has been also reported in other studies.[53, 54]Thermal decomposition of all the HIPEs was occurred above 175 ^{o}C (Figure S11), demonstrating that the HIPEs have sufficient thermal stability for use as the SPEs in lithium batteries even at the elevated temperature.

Figure 7 shows DSC thermograms of HIPEs. The T_gs of PEOEC segments in

HIPEs are larger than those of PEOEC electrolytes (Figure 3 and Figure S7). This indicates that the semi-interpenetrating network structure of HIPEs restricts the PEOEC chain mobility, although it enhances the dimensional stability of electrolytes to form flexible free-standing films (Scheme 2). The L-HIPEs have smaller T_g values than H-HIPEs, because L-PEOEC electrolyte in L-HIPEs has higher chain mobility than H-PEOEC electrolyte in H-HIPEs due to its lower molecular weight (Figure 3 and Figure S7). As OA-POSS content increases, T_g values gradually decrease for both HIPEs and L-HIPEs. It has been known that the changes in T_g of polymers containing POSS moieties are mainly attributed to two factors. One is the rigidity of POSS, which decreases the mobility of the chains, resulting in an increase of T_g.[35, 36] The other is the increase of free volume in polymers due to the large volume of POSS, which can lower T_g by internal plasticization.[38, 55 56]In the case of HIPEs, the combined effect of these two competing factors led to an decrease in the T_g values. We also believe that the semi-interpenetrating network structure consisting of free PEOEC chains and cross-linked OA-POSS/ETPTA network could affect the changes of T_g, because

the PEOEC chains in HIPEs are not directly connected by covalent bonds to the OA-POSS/ETPTA cross-linked network. In addition, as the OA-POSS has smaller acrylic C=C bonds than ETPTA, the decrease in cross-linking density in HIPEs with increasing OA-POSS content might also affect the decrease in T_g. It is noteworthy that the HIPEs with larger POSS content have lower T_g than HIPEs with smaller POSS content, but they can form free-standing electrolyte films having higher modulus.

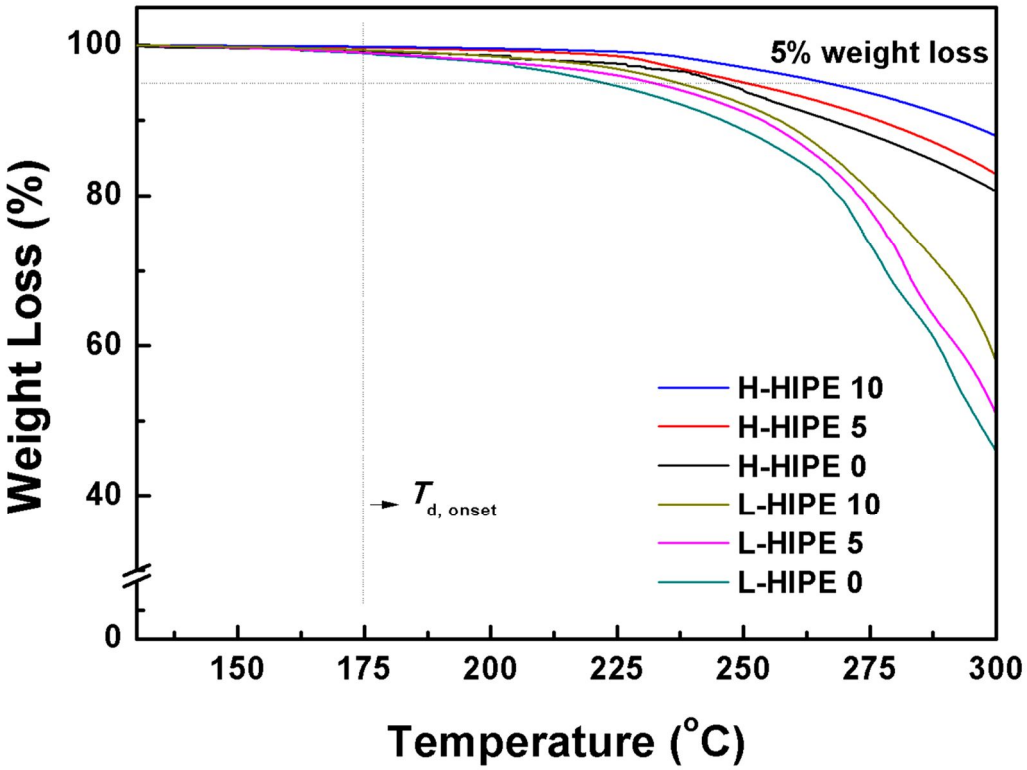

Figure S11. TGA curves of H-HIPEs and L-HIPEs.

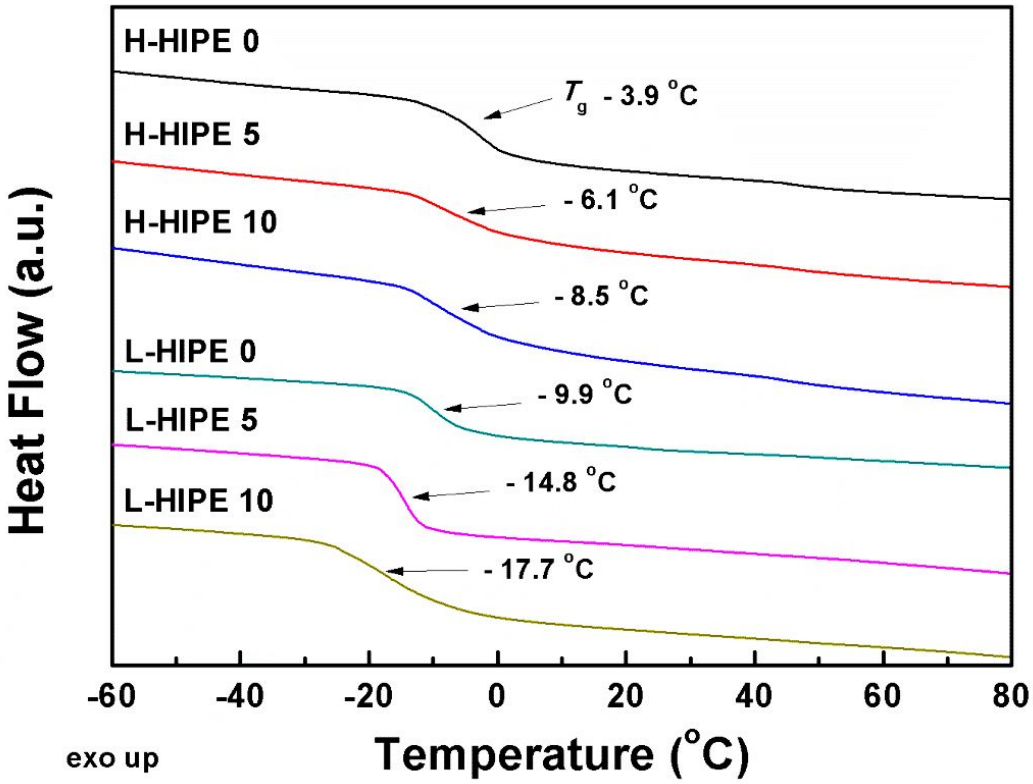

Figure 7. DSC Curves of HIPEs.

3.7.Ionic Conductivity of HIPEs.

The ionic conductivities of HIPEs are presented in Figure 8. The ionic conductivity of HIPEs increases as the content of OA-POSS in HIPEs increases (Figure 8(a)). The increase in ionic conductivity of HIPEs with increasing OA-POSS content in HIPEs should be attributed to the smaller T_g values (Figure 6). A low T_g value is a key factor to achieve high ionic conductivity of SPEs, because lithium ions in polymer matrix are transferred by the segmental motion of polymer chains.[4] Therefore, it was found that the introduction of OA-POSS into the HIPEs can enhance the dimensional stability of HIPEs due to its reinforcing effect and that it can simultaneously enhance the ionic conductivity of HIPEs by increasing the mobility of ion-conducting PEOEC segments. Furthermore, higher ionic conductivities could be obtained from the HIPEs when they contain lower molecular weight PEOEC. The higher chain mobility of L-HIPEs, as expected by the lower T_g, should provide the higher ionic conductivities than H-HIPEs (Figure 6). Among the HIPEs, the L-HIPE10 exhibits the highest ionic conductivity;

3.74×10^{-5} and 3.26×10^{-4} S cm^{-1} at 30 and 60 ^{o}C, respectively. The obtained ionic conductivity value for L-HIPE10 is nearly 2 orders of magnitude larger than that for conventional SPEs based on the high molecular weight PEO homopolymer.[6, 57] The value was found to be even higher than that of low molecular weight PEO electrolyte characterized in this study (Figure S5).

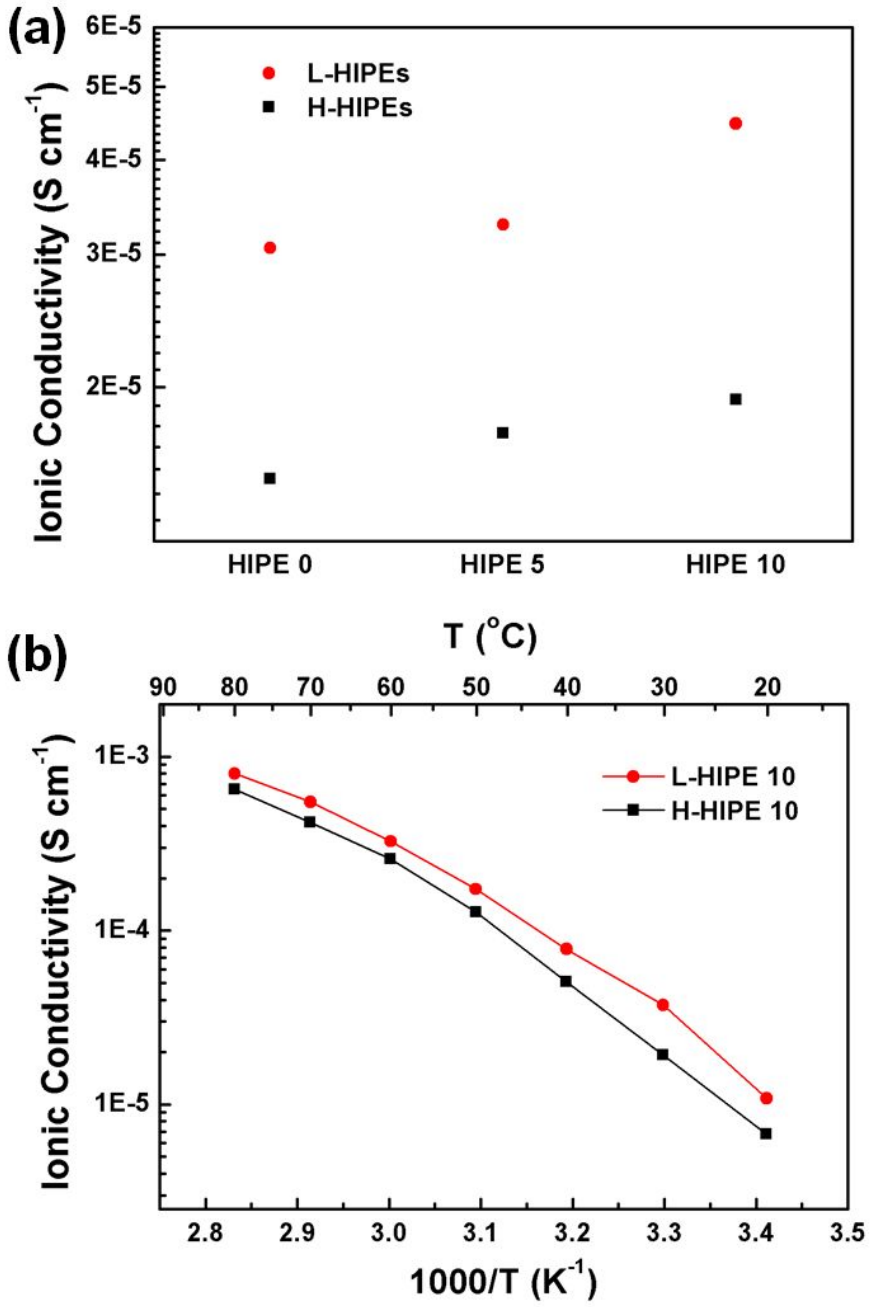

Figure 8. (a) Ionic Conductivities of HIPEs at 30°C and (b) Temperature dependence of ionic conductivities of L-HIPE10 and H-HIPE10.

3.8.Electrochemical Performance of L-HIPE10.

We investigated the electrochemical stability and all-solid-state battery performance using L-HIPE10 which has the highest ionic conductivity among the HIPEs. Lithium trifluoromethanesulfonate ($LiSO_3CF_3$) was used as lithium salt in L-HIPE10 for the electrochemical analyses, because it is known that the stability of $LiClO_4$ is not enough to be applied for high temperature operation of batteries.[58] The ionic conductivity of L-HIPE10 with $LiSO_3CF_3$ was found to be close to that with $LiClO_4$ (Figure S12). Figure 9 shows linear sweep voltammograms of the stainless steel / L-HIPE10 / lithium metal cells at both 25 and 60 ^oC. The anodic currents from oxidation of L-HIPE10 were observed at voltages higher than about 5.0 and 4.7 V at 25 and 60 ^oC, respectively. When temperature increases from 25 to 60 ^oC, the potential window decreases by 0.3 V and the oxidation current increases.[59] However, the L-HIPE10 still can be applied to 4 V class lithium batteries even at elevated temperatures. The potential window of L-HIPE10 is comparable to or slightly wider than that of the conventional

linear PEO-based electrolyte.[60] Moreover, it is higher than that of the currently used organic liquid electrolyte (~4.5 V at 25 ^{o}C), demonstrating a better electrochemical stability of the electrolyte over a wide temperature range.[61, 62]

All-solid-state lithium cell of V_2O_5 / L-HIPE10 / lithium metal was fabricated, and the charge-discharge capacities were investigated. The L-HIPE10 film has enough dimensional stability to separate the electrodes in the cell; no short circuit was found during the test. Thus, we did not use the separator to assemble the cells in this study, in contrast to lithium ion batteries containing liquid electrolytes. Figure 10(a) shows the charge-discharge curves of the V_2O_5 / L-HIPE10 / lithium metal cells at 60°C in the potential range of 2– 4 V. The cell delivers a specific discharge capacity higher than 280 mAh g^{-1} at the initial cycle, which is close to the theoretical discharge capacity of V_2O_5 in this potential region (294 mAh g^{-1}). The discharge capacity is retained almost stable over 30 cycles as shown in Figure 10(b). These preliminary results clearly reveal the possible applications of the L-HIPE10 as solid-state electrolytes for lithium batteries. It should be also noted that the cell with L-HIPE10 can be stably operated at the elevated temperatures, at

which the cell with liquid electrolytes generally exhibit poor performance due to their volatility and low potential windows.[3, 63] The detailed electrochemical investigation of all-solid-state batteries with L-HIPE10 will be the subject of future studies.

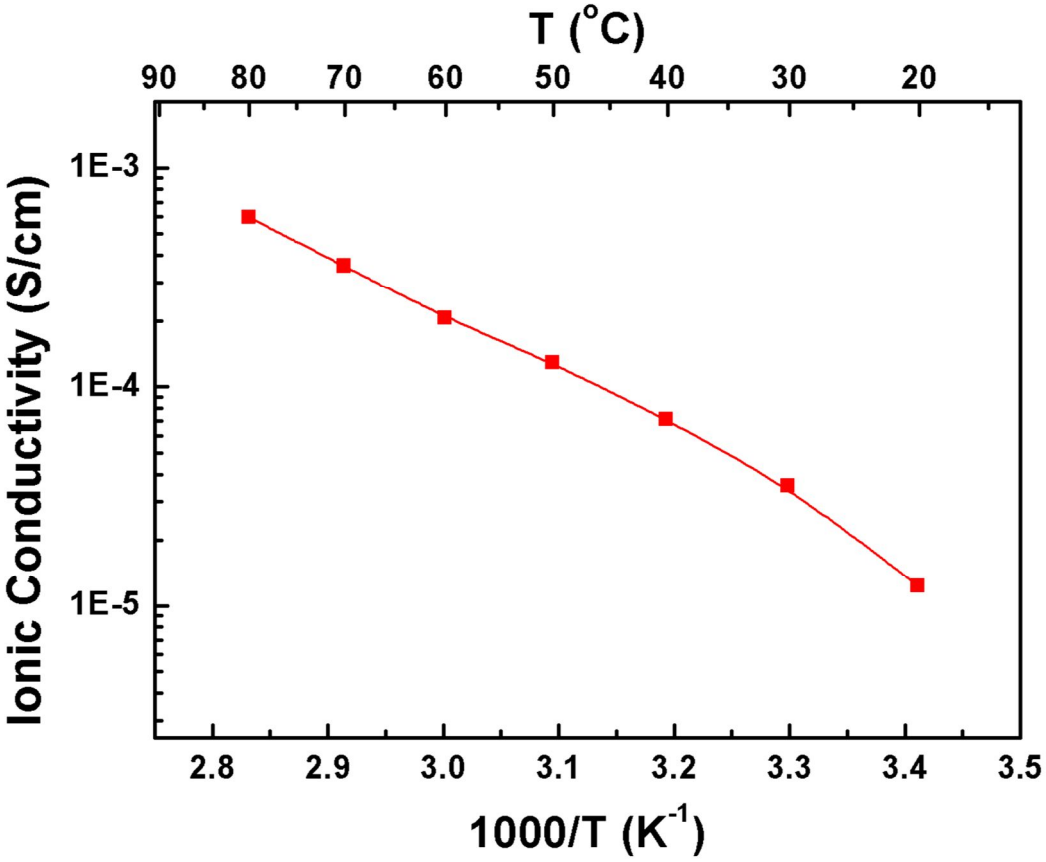

Figure S12. Temperature dependence of ionic conductivity of L-HIPE10 with $LiSO_3CF_3$ ([Li] / ([EO] + [EC]) = 0.15).

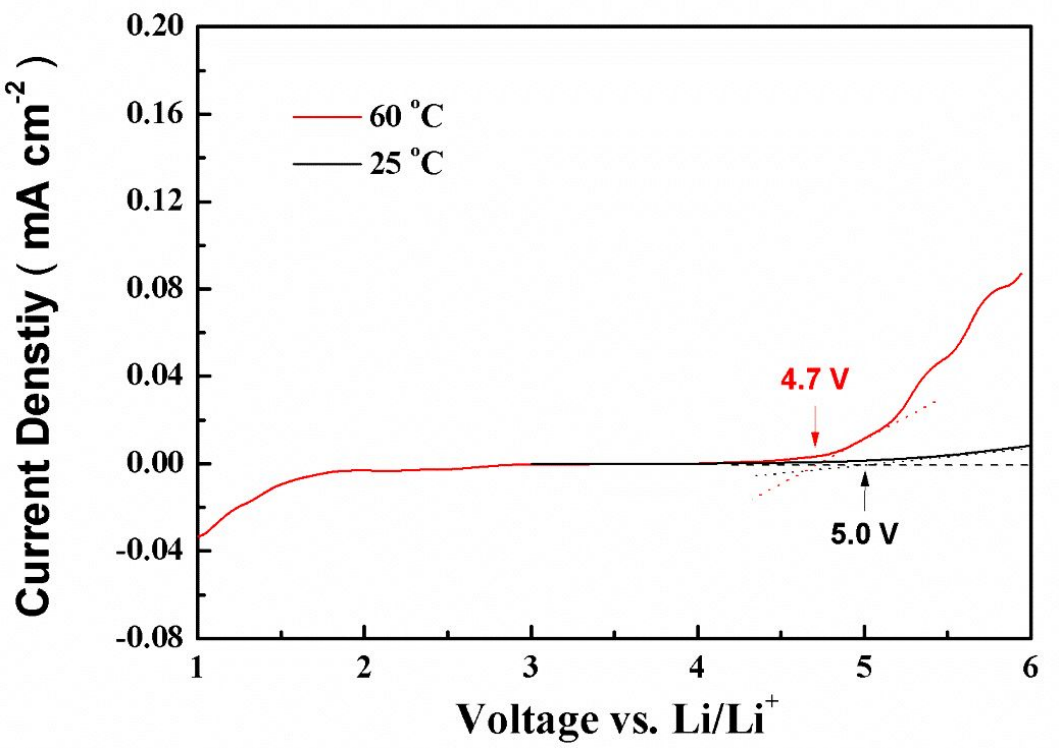

Figure 9. Linear Sweep Voltamograms of Stainless Steel Electrodes in L-HIPE10 with $LiSO_3CF_3$ at 25 °C and 60 °C.

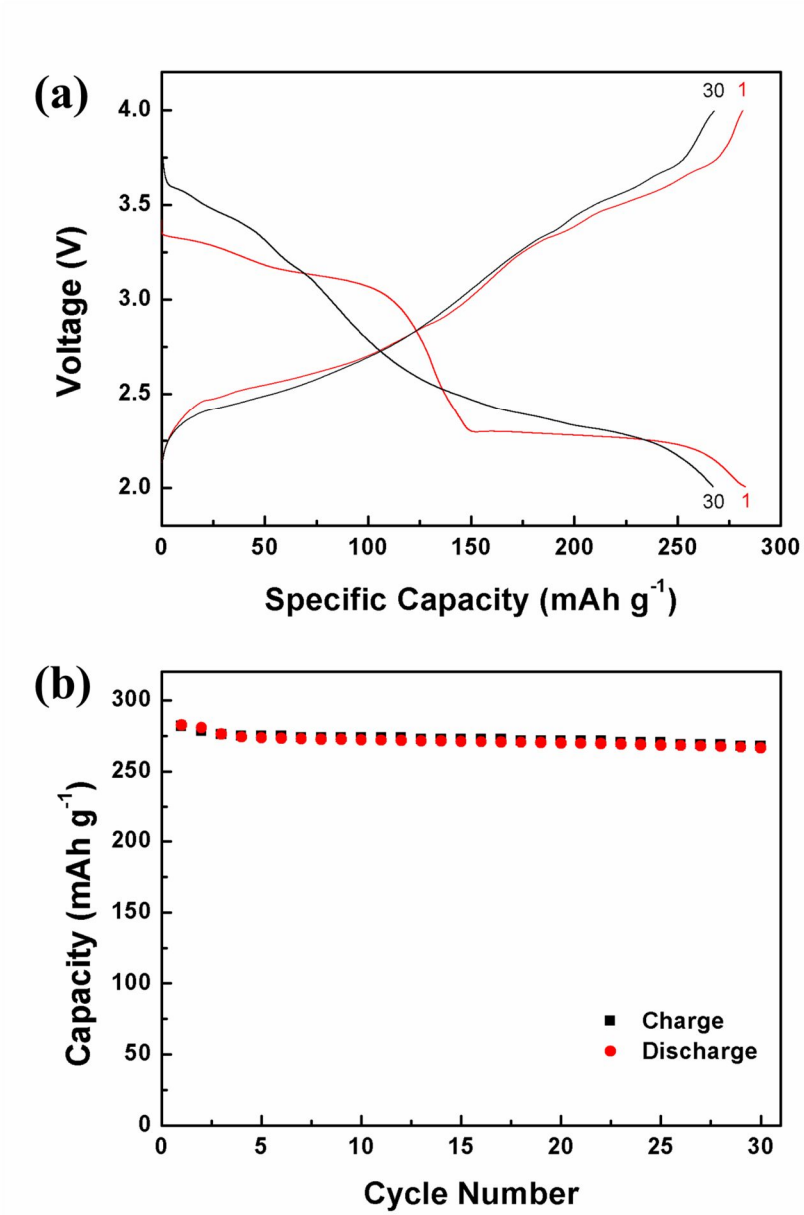

Figure 10. (a) Charge-Discharge Curves and (b) Discharg capacity *vs.* Cycle Behaviors of All-Solid-State Li / L-HIPE10 (with $LiSO_3CF_3$) / V_2O_5 cell measured at 60 ^oC.

4. Conclusion

We have prepared a series of organic/inorganic hybrid semi-interpenetrating network electrolytes (HIPEs) based on poly(ethylene oxide-*co*-ethylene carbonate) (PEOEC) to investigate the effect of OA-POSS content on the properties of the electrolytes including dimensional stability and ionic conductivity. The PEOEC was used as lithium ion-conducting polymers in HIPEs, because the PEOEC electrolyte was found to exhibit higher ionic conductivity than PEO electrolyte when doped with lithium salt. The high ionic conductivity of PEOEC electrolyte is due to the polar EC units in PEOEC, which can suppress the crystallinity of EO segments in the polymers and increase the dissociation of lithium salt. The incorporation of OA-POSS into the HIPEs not only increases the ionic conductivity by increasing free volume, but also enhances the dimensional stability due to its reinforcement effect. The highest conductivities were achieved when the HIPEs have largest OA-POSS content and lower molecular weight PEOEC and the values are 3.74×10^{-5} and 3.26×10^{-4} S cm^{-1} at 30 and 60 ^{o}C,

respectively. The HIPEs are electrochemically stable up to 4.7 V even at 60 ^{o}C, suggesting that they are applicable to the 4 V class lithium ion batteries over a wide temperature range. We have shown that the all-solid-state lithium cell with HIPEs exhibits a high specific capacity and good cycle performance at 60 ^{o}C, demonstrating the possible application of HIPEs as SPEs for lithium batteries. We expect that our results will provide insight into the utilization of PEOEC and organic/inorganic hybrid interpenetrating network structures for SPE applications.

5. References

1. Tarascon, J.M. & Armand, M. Issues and challenges facing rechargeable lithium batteries. *Nature* **414**, 359-367 (2001).
2. Scrosati, B. Power sources for portable electronics and hybrid cars: lithium batteries and fuel cells. *The Chemical Record* **5**, 286-297 (2005).
3. Scrosati, B. & Garche, J. Lithium batteries: Status, prospects and future. *Journal of Power Sources* **195**, 2419-2430 (2010).
4. Meyer, W.H. Polymer Electrolytes for Lithium-Ion Batteries. *Advanced Materials* **10**, 439-448 (1998).
5. Manuel Stephan, A. & Nahm, K.S. Review on composite polymer electrolytes for lithium batteries. *Polymer* **47**, 5952-5964 (2006).
6. Fenton, D.E., Parker, J.M. & Wright, P.V. Complexes of alkali metal ions with poly(ethylene oxide). *Polymer* **14**, 589 (1973).
7. Li, Q. et al. Interface properties between a lithium metal electrode and a poly(ethylene oxide) based composite polymer electrolyte. *Journal of Power Sources* **94**, 201-205 (2001).
8. Michael, M.S., Jacob, M.M.E., Prabaharan, S.R.S. & Radhakrishna, S. Enhanced lithium ion transport in PEO-based solid polymer electrolytes employing a novel class of plasticizers. *Solid State Ionics* **98**, 167-174 (1997).
9. Shieh, Y.-T., Liu, G.-L., Hwang, K.C. & Chen, C.-C. Crystallization, melting and morphology of PEO in PEO/MWNT-g-PMMA blends. *Polymer* **46**, 10945-10951 (2005).
10. Park, S.-J., Han, A.R., Shin, J.-S. & Kim, S. Influence of crystallinity on ion conductivity of PEO-based solid electrolytes for lithium batteries.

Macromolecular Research **18**, 336-340 (2010).

11. Kakihana, M., Schantz, S. & Torell, L.M. Raman spectroscopic study of ion–ion interaction and its temperature dependence in a poly(propylene-oxide)-based NaCF3SO3 –polymer electrolyte. *The Journal of Chemical Physics* **92**, 6271-6277 (1990).
12. Schantz, S., Torell, L.M. & Stevens, J.R. Ion pairing effects in poly(propylene glycol)–salt complexes as a function of molecular weight and temperature: A Raman scattering study using NaCF3SO3 and LiClO4. *The Journal of Chemical Physics* **94**, 6862-6867 (1991).
13. Ferry, A. Ionic interactions and transport properties in methyl terminated poly(propylene glycol)(4000) complexed with LiCF3SO3. *Journal of Physical Chemistry B* **101**, 150-157 (1997).
14. Ferry, A., Jacobsson, P. & Torell, L.M. The molar conductivity behavior in polymer electrolytes at low salt concentrations; A Raman study of poly(propylene glycol) complexed with LiCF3SO3. *Electrochimica Acta* **40**, 2369-2373 (1995).
15. Forsyth, M., Tipton, A.L., Shriver, D.F., Ratner, M.A. & MacFarlane, D.R. Ionic conductivity in poly(diethylene glycol-carbonate)/sodium triflate complexes. *Solid State Ionics* **99**, 257-261 (1997).
16. Xu, W., Belieres, J.P. & Angell, C.A. Ionic conductivity and electrochemical stability of poly[oligo(ethylene glycol)oxalate]-lithium salt complexes. *Chemistry of Materials* **13**, 575-580 (2001).
17. Lee, J.C. & Litt, M.H. Ring-opening polymerization of ethylene carbonate and depolymerization of poly(ethylene oxide-co-ethylene carbonate). *Macromolecules* **33**, 1618-1627 (2000).
18. Jeon, J.D., Kim, M.J. & Kwak, S.Y. Effects of addition of TiO2 nanoparticles on mechanical properties and ionic conductivity of solvent-

free polymer electrolytes based on porous P(VdF-HFP)/P(EO-EC) membranes. *Journal of Power Sources* **162**, 1304-1311 (2006).

19. Jeon, J.D. & Kwak, S.Y. Pore-filling solvent-free polymer electrolytes based on porous P(VdF-HFP)/P(EO-EC) membranes for rechargeable lithium batteries. *Journal of Membrane Science* **286**, 15-21 (2006).
20. Elmér, A.M. & Jannasch, P. Synthesis and characterization of poly(ethylene oxide-co-ethylene carbonate) macromonomers and their use in the preparation of crosslinked polymer electrolytes. *Journal of Polymer Science Part A: Polymer Chemistry* **44**, 2195-2205 (2006).
21. Capuano, F., Croce, F. & Scrosati, B. Composite Polymer Electrolytes. *Journal of the Electrochemical Society* **138**, 1918-1922 (1991).
22. Tominaga, Y., Asai, S., Sumita, M., Panero, S. & Scrosati, B. A novel composite polymer electrolyte: Effect of mesoporous SiO2 on ionic conduction in poly(ethylene oxide)-LiCF3SO3 complex. *Journal of Power Sources* **146**, 402-406 (2005).
23. Soo, P.P. et al. Rubbery block copolymer electrolytes for solid-state rechargeable lithium batteries. *Journal of the Electrochemical Society* **146**, 32-37 (1999).
24. Panday, A. et al. Effect of Molecular Weight and Salt Concentration on Conductivity of Block Copolymer Electrolytes. *Macromolecules* **42**, 4632-4637 (2009).
25. Jeon, J.D., Kwak, S.Y. & Cho, B.W. Solvent-free polymer electrolytes - I. Preparation and characterization of polymer electrolytes having pores filled with viscous P(EO-EC)/LiCF3SO3. *Journal of the Electrochemical Society* **152**, A1583-A1589 (2005).
26. He, D., Cho, S.Y., Kim, D.W., Lee, C. & Kang, Y. Enhanced ionic conductivity of semi-IPN solid polymer electrolytes based on star-shaped

oligo(ethyleneoxy)cyclotriphosphazenes. *Macromolecules* **45**, 7931-7938 (2012).

27. Basak, P. & Manorama, S.V. PEO-PU/PAN semi-interpenetrating polymer networks for SPEs: influence of physical properties on the electrical characteristics. *Solid State Ionics* **167**, 113-121 (2004).
28. Tran-Van, F. et al. Self-supported semi-interpenetrating polymer networks for new design of electrochromic devices. *Electrochimica Acta* **53**, 4336-4343 (2008).
29. Ha, H.-J. et al. UV-curable semi-interpenetrating polymer network-integrated, highly bendable plastic crystal composite electrolytes for shape-conformable all-solid-state lithium ion batteries. *Energy & Environmental Science* **5**, 6491-6499 (2012).
30. Marques, R.S. et al. Synthesis and characterization of semi-interpenetrating networks based on poly(dimethylsiloxane) and poly(vinyl alcohol). *Journal of Applied Polymer Science* **115**, 158-166 (2010).
31. Rohman, G., Grande, D., Lauprêtre, F., Boileau, S. & Guérin, P. Design of Porous Polymeric Materials from Interpenetrating Polymer Networks (IPNs): Poly(dl-lactide)/Poly(methyl methacrylate)-Based Semi-IPN Systems. *Macromolecules* **38**, 7274-7285 (2005).
32. He, D., Kim, D.W., Park, J.S., Cho, S.Y. & Kang, Y. Electrochemical properties of semi-interpenetrating polymer network solid polymer electrolytes based on multi-armed oligo(ethyleneoxy) phosphate. *Journal of Power Sources* **244**, 170-176 (2013).
33. Tan, B.H. et al. Tuning self-assembly of hybrid PLA-P(MA-POSS) block copolymers in solution via stereocomplexation. *Polymer Chemistry* **4**, 1250-1259 (2013).
34. Wang, F., Lu, X. & He, C. Some recent developments of polyhedral

oligomeric silsesquioxane (POSS)-based polymeric materials. *Journal of Materials Chemistry* **21**, 2775-2782 (2011).

35. Ryu, H.-S., Kim, D.-G. & Lee, J.-C. Polysiloxanes containing polyhedral oligomeric silsesquioxane groups in the side chains; synthesis and properties. *Polymer* **51**, 2296-2304 (2010).
36. Ryu, H.S., Kim, D.G. & Lee, J.C. Synthesis and properties of polysiloxanes containing polyhedral oligomeric silsesquioxane (POSS) and oligo (ethylene oxide) groups in the side chains. *Macromolecular Research* **18**, 1021-1029 (2010).
37. Dong, F. & Ha, C.S. Multifunctional materials based on polysilsesquioxanes. *Macromolecular Research* **20**, 335-343 (2012).
38. Wu, J., Haddad, T.S. & Mather, P.T. Vertex Group Effects in Entangled Polystyrene-Polyhedral Oligosilsesquioxane (POSS) Copolymers. *Macromolecules* **42**, 1142-1152 (2009).
39. Kim, D.G., Sohn, H.S., Kim, S.K., Lee, A. & Lee, J.C. Star-shaped polymers having side chain poss groups for solid polymer electrolytes; synthesis, thermal behavior, dimensional stability, and ionic conductivity. *Journal of Polymer Science Part a-Polymer Chemistry* **50**, 3618-3627 (2012).
40. Kim, D.-G. et al. Preparation of solid-state composite electrolytes based on organic/inorganic hybrid star-shaped polymer and PEG-functionalized POSS for all-solid-state lithium battery applications. *Polymer* **54**, 5812-5820 (2013).
41. Niitani, T., Amaike, M., Nakano, H., Dokko, K. & Kanamura, K. Star-Shaped Polymer Electrolyte with Microphase Separation Structure for All-Solid-State Lithium Batteries. *Journal of the Electrochemical Society* **156**, A577-A583 (2009).

42. Watanabe, M., Suzuki, Y. & Nishimoto, A. Single ion conduction in polyether electrolytes alloyed with lithium salt of a perfluorinated polyimide. *Electrochimica Acta* **45**, 1187-1192 (2000).
43. Pan, Y.-C. et al. Synthesis and characterization of a new hyperbranched organic–inorganic solid polymer electrolyte with cyanuric chloride as a core element. *Electrochimica Acta* **56**, 8519-8529 (2011).
44. Albinsson, I., Mellander, B.E. & Stevens, J.R. Ion association effects and ionic conductivity in polymer electrolytes. *Solid State Ionics* **60**, 63-66 (1993).
45. Yang, J., Gao, J., Du, Y. & Liu, X. Rheology and Mechanical Properties of PVC/Acrylonitrile–Chlorinated Polyethylene-Styrene/MAP-POSS Nanocomposites. *Polymer-Plastics Technology and Engineering* **52**, 820-826 (2013).
46. Ren, J. et al. A novel crosslinking organic–inorganic hybrid proton exchange membrane based on sulfonated poly(arylene ether sulfone) with 4-amino-phenyl pendant group for fuel cell application. *Journal of Membrane Science* **434**, 161-170 (2013).
47. Zuo, X. et al. Enhanced performance of a novel gel polymer electrolyte by dual plasticizers. *Journal of Power Sources* **239**, 111-121 (2013).
48. Pan, H. & Qiu, Z. Biodegradable Poly(l-lactide)/Polyhedral Oligomeric Silsesquioxanes Nanocomposites: Enhanced Crystallization, Mechanical Properties, and Hydrolytic Degradation. *Macromolecules* **43**, 1499-1506 (2010).
49. Fukae, R., Yoshimura, M., Yamamoto, T. & Nishinari, K. Effect of stereoregularity and molecular weight on the mechanical properties of poly(vinyl alcohol) hydrogel. *Journal of Applied Polymer Science* **120**, 573-578 (2011).

50. Siengchin, S. & Abraham, T.N. Morphology and rheological properties of high density polyethylene/fluorothermoplastics blends. *Journal of Applied Polymer Science* **127**, 919-925 (2013).
51. Soo, P.P. et al. Rubbery block copolymer electrolytes for solid-state rechargeable lithium batteries. *Journal of the Electrochemical Society* **146**, 32-37 (1999).
52. Calahorra, M.E., Cortázar, M., Eguiazábal, J.I. & Guzmán, G.M. Thermogravimetric analysis of cellulose: Effect of the molecular weight on thermal decomposition. *Journal of Applied Polymer Science* **37**, 3305-3314 (1989).
53. Hoque, M.A., Kakihana, Y., Shinke, S. & Kawakami, Y. Polysiloxanes with Periodically Distributed Isomeric Double-Decker Silsesquioxane in the Main Chain. *Macromolecules* **42**, 3309-3315 (2009).
54. Liu, H., Zheng, S. & Nie, K. Morphology and Thermomechanical Properties of Organic−Inorganic Hybrid Composites Involving Epoxy Resin and an Incompletely Condensed Polyhedral Oligomeric Silsesquioxane. *Macromolecules* **38**, 5088-5097 (2005).
55. Pistor, V., Ornaghi, F.G., Ornaghi, H.L. & Zattera, A.J. Dynamic mechanical characterization of epoxy/epoxycyclohexyl–POSS nanocomposites. *Materials Science and Engineering: A* **532**, 339-345 (2012).
56. Brus, J., Urbanova, M. & Strachota, A. Epoxy Networks Reinforced with Polyhedral Oligomeric Silsesquioxanes: Structure and Segmental Dynamics as Studied by Solid-State NMR. *Macromolecules* **41**, 372-386 (2007).
57. Kelly, I.E., Owen, J.R. & Steele, B.C.H. Poly(ethylene oxide) electrolytes for operation at near room temperature. *Journal of Power Sources* **14**, 13-

21 (1985).

58. Aravindan, V., Gnanaraj, J., Madhavi, S. & Liu, H.K. Lithium-ion conducting electrolyte salts for lithium batteries. *Chemistry - A European Journal* **17**, 14326-14346 (2011).

59. Lin, Y. et al. A wider temperature range polymer electrolyte for all-solid-state lithium ion batteries. *RSC Advances* **3**, 10722-10730 (2013).

60. Armand, M.B., Duclot, M.J. & Rigaud, P. Polymer solid electrolytes: Stability domain. *Solid State Ionics* **3–4**, 429-430 (1981).

61. Hallinan, D.T. & Balsara, N.P. Polymer Electrolytes. *Annual Review of Materials Research, Vol 43* **43**, 503-+ (2013).

62. Wang, S.-H., Hou, S.-S., Kuo, P.-L. & Teng, H. Poly(ethylene oxide)-co-Poly(propylene oxide)-Based Gel Electrolyte with High Ionic Conductivity and Mechanical Integrity for Lithium-Ion Batteries. *ACS Applied Materials & Interfaces* **5**, 8477-8485 (2013).

63. Liu, Y., Cai, Z., Tan, L. & Li, L. Ion exchange membranes as electrolyte for high performance Li-ion batteries. *Energy & Environmental Science* **5**, 9007-9013 (2012).

국문 요약

PEOEC를 기반으로하는 유무기복합 준상호침투형 가교구조의 고분자 전해질 막을 합성하였고 이를 리튬 이차전지의 고체상 고분자 전해질로 응용하였다. 무정형구조를 가지면서 높은 유전상수 값을 나타내는 PEOEC의 분자량에 따른 이온전도도 효과를 알아보기 위하여 두 종류의 PEOEC를 합성하여 이온전달체로 사용해주었다. 또한 POSS의 도입으로 인한 물성 및 전해질의 특성 변화를 체계적으로 알아보고자 가교가능단량체로 사용해준 ETPTA대 POSS의 비율을 변화시켜가며 다양한 막을 합성하였다. 그 결과 POSS 단량체가 전체 질량대비 10wt% 함유되어있고, 분자량이 작은 PEOEC고분자를 이온전달체로 사용해준 L-HIPE10전해질 막이 가장 우수한 이온전도도 특성을 보였다. 이는 분자량이 작은 이온전달체 일수록 사슬의 유동성이 좋기 때문이며, 또한 부피가 큰 POSS가 도입되면서 자유부피를 증가시켜주는 효과가 있기 때문이다. L-HIPE 10전해질 막을 별도의 분리막을 사용하지 않은 전 고체상 리튬이차전지 cell에 적용한 결과 60°C 고온

에서도 안정적으로 작동하였고, 이를 통해 실제 전고체상 리튬이차전지용 전해질 막으로 응용가능성을 확인하였다.

주요어: 전고체상 배터리, 유무기 복합 전해질, POSS, 준상호침투형 가교구조, 에틸렌옥사이드-에틸렌카보네이트 공중합체